The unfolded protein response in grapevine: abiotic and biotic stresses induce the expression of VvbZIP60, VvbZIP17, VvBIP3, and VvIRE1

Tania Marzari[1], Cécile Blanchard[1], Emma Poilvert[1], Karine Palavioux[1], Agnès Klinguer[1], Alix Martinez[1], Aurélien Henry[1], Benoit Poinssot[1], Mathieu Gayral[1*]

[1] Université Bourgogne Europe, Institut Agro, INRAE, UMR Agroécologie, 21000 DIJON, FRANCE.

[*]Corresponding Author: Mathieu Gayral (mathieu.gayral@inrae.fr)

ORCID & email addresses:

Tania Marzari:	tania.marzari@inrae.fr	https://orcid.org/0009-0006-0584-8475
Cécile Blanchard:	cecile.blanchard@u-bourgogne.fr	
Emma Poilvert:	emma.poilvert@inrae.fr	https://orcid.org/0009-0005-1502-9468
Karine Palavioux:	karine.palavioux@inrae.fr	
Agnès Klinguer:	agnes.klinguer@inrae.fr	
Aurélien Henry:	aurelien.henry@inrae.fr	
Alix Martinez:	alix.martinez@inrae.fr	
Benoit Poinssot:	benoit.poinssot@inrae.fr	https://orcid.org/0000-0001-5890-4318
Mathieu Gayral:	mathieu.gayral@inrae.fr	https://orcid.org/0000-0001-5760-1622

Word count: 6855 Number of figures: 7 Number of Tables: 0 Sup. Data: 9

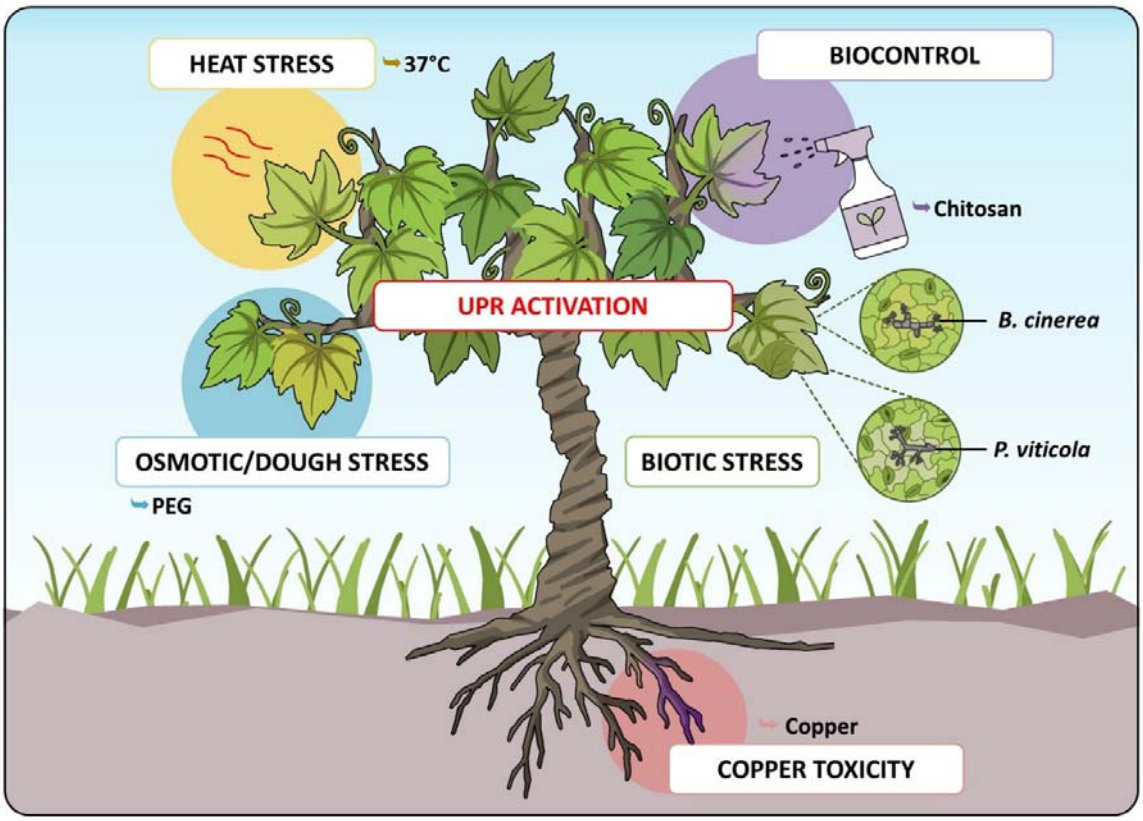

Graphical abstract

Abstract

A wide range of stresses can lead to the accumulation of unfolded or misfolded proteins in the lumen of the endoplasmic reticulum (ER), a condition known as ER stress. To restore proteostasis, eukaryotic cells activate a signaling network called the unfolded protein response (UPR). In *Vitis vinifera*, two arms of the UPR have been identified: the IRE1/bZIP60 arm and the bZIP17 arm. Notably, no putative ortholog of bZIP28 has been found in *V. vinifera*, whereas this is the case for *Brassicaceae* species. We demonstrated that *VvbZIP60* undergoes unconventional splicing upon treatment with dithiothreitol (DTT) and tunicamycin (TM), both classical ER stress inducers. Moreover, after testing several abiotic factors, we observed a strong transcriptional activation of UPR-related genes in response to heat and osmotic stresses, as well as copper exposure. Grapevine is also subject to a broad range of microbial challenges, including pathogens such as *Plasmopara viticola* and *Botrytis cinerea*. Both pathogens triggered UPR genes activation in grapevine leaves and berries. Interestingly, *VvbZIP17* was also upregulated in green berries, a developmental stage associated with strong basal resistance to *B. cinerea*. Collectively, these findings suggest that the IRE1/bZIP60 and bZIP17 arms of the UPR are not only structurally conserved in grapevine but are also transcriptionally responsive to a variety of abiotic and biotic stresses.

Keywords: Heat/osmotic stress; downy mildew; grey mould; RTqPCR

1. Introduction

Grapevine cultivation is one of the most significant agricultural activities worldwide, it covers approximately 7.2 million hectares of the total rural surface and holds immense economic weight on the international market generating over 36 billion euros in wine production, estimated to be around 240 million hectoliters (OIV, International Organisation of Vine and Wine, 2023). However, this sector faces increasing challenges due to extreme climatic conditions and fungal diseases, which have significantly affected yield and fruit quality. As a perennial crop, grapevine growth relies on stable climatic conditions, including optimal temperatures, adequate water supply and frost-free periods (Palliotti and Poni, 2015; Zapata et al., 2017). Unfortunately, maintaining these conditions is becoming increasingly difficult, thereby raising the challenges of grapevine cultivation.

Plants have evolved a range of tolerance mechanisms to cope with both abiotic and biotic stress conditions and the unfolded protein response (UPR) is one of them. Acting as a sentinel for adverse conditions, the UPR pathway allows the maintaining of cellular homeostasis controlling protein folding and limiting accumulation of misfolded and/or unfolded proteins in the endoplasmic reticulum (ER) (Howell, 2013). The adaptation to changing conditions or pathogen attacks triggers extensive transcriptional reprogramming, which can overwhelm the ER's capacity to manage protein folding properly. Notably, environmental factors including heat, salt or drought (Liu et al., 2007; Valente et al., 2009; Deng et al., 2011) and microorganism interactions (Moreno et al., 2012; Gayral et al., 2020; Qiang et al., 2021; Blanchard et al., 2025) can intensify the workload of the ER beyond its capacity. This leads to the accumulation of misfolded and unfolded proteins within the ER lumen, a condition referred as ER stress (Howell, 2013). In response to this accumulation, the ER activates the UPR pathway to balance its protein-folding and degradation capacities with the cell's needs (Walter and Ron, 2011). When managed effectively, short-term ER stress can be alleviated, allowing the ER machinery to recover. However, if ER stress persists, it can lead to autophagy, programmed cell death (PCD) or even the death of the entire plant (Iwata and Koizumi, 2005; Yang et al., 2014).

In plants, two arms of the UPR pathway have been describes in the model plant *Arabidopsis thaliana,* the ER-transmembrane inositol-requiring enzyme 1 (IRE1) / basic leucin zipper 60 (bZIP60) arm and the membrane-associated transcription factors (TFs) bZIP17/bZIP28 arm (Liu et al., 2007; Nagashima et al., 2011; Hollien, 2013; Howell, 2013). Interestingly, in the *A. thaliana* genome, three isoforms of IRE have been described: AtIRE1A, AtIRE1B and AtIRE1C (Deng et al., 2011; Koizumi et al., 2001). While AtIRE1C is primarily involved in development and gametogenesis (Mishiba et al., 2019; Pu et al., 2019), AtIRE1A and AtIRE1B are particularly active during ER stress to mediate the unconventional splicing of bZIP60 mRNA resulting in a 23-pb

elimination and a 3' frameshift, encoding an UPR-specific TF lacking its transmembrane domain and presenting an additional nuclear localization signal (NLS). The translated spliced form of AtbZIP60 (bZIP60s) is then translocated to the nucleus, where it activates downstream UPR responsive genes (Nagashima et al., 2011; Deng et al., 2011). In *A. thaliana*, the unconventional splicing of bZIP60 mRNA is incomplete, with the unspliced form (bZIP60us) consistently present in high amounts. Depending on stress conditions, the splicing reaches its peak between 0.5 and 2 hours, after which the level of bZIP60 decreases (Parra-Rojas et al., 2015). The IRE1 activation occurs through conformational changes triggered by lateral oligomerization in the ER membrane. While several models explain IRE1 dimerization in yeast and mammals, the mechanisms in plants remain unclear. One model suggests that BIP (binding protein), a predominant ER-resident Hsp70 chaperone normally associated with IRE1, is released under ER stress allowing IRE1 self-dimerization thus initiating the bZIP60 splicing (Bertolotti et al., 2000; Kimata et al., 2003). Another model proposes that IRE1's luminal domain directly interacts with unfolded proteins (Gardner and Walter, 2011). Nowadays, the components of the IRE1-bZIP60 pathway and the splicing process have been identified in the model plant Arabidopsis and few other crop species, notably after treatment with ER stress inducers such as tunicamycin (TM) and dithiothreitol (DTT) which inhibit glycosylation and disulfide bond formation, respectively (Deng et al., 2011; Nagashima et al., 2011; Hayashi et al., 2012). IRE1 has also another function, called Regulated IRE1-Dependent RNA Decay (RIDD), which degrades other mRNAs associated with ribosomes on the ER membrane (Li and Howell, 2021).

The second arm of the UPR pathway is mediated by the ER membrane-associated TFs bZIP17 and bZIP28 in *A. thaliana*. Under non-stress conditions, the luminal domain of AtbZIP28 is associated with BIP chaperone proteins (Srivastava et al., 2013). Under stress conditions, AtbZIP28 dissociates from BIP, and along with AtbZIP17, is translocated to the Golgi apparatus, where it undergoes sequential cleavage by site-1 protease (S1P) and site-2 protease (S2P). Cleavage by S2P releases the N-terminal domain of bZIP17/bZIP28, allowing their relocation to the nucleus to activate stress-responsive gene expression (Liu et al., 2007). However, the exact mechanisms for the activation of this UPR arm remain under investigation. For example, studies suggest that AtS1P may not be essential for activating AtbZIP28 (Iwata and Koizumi, 2005) and there is no direct evidence at bZIP17/BIP association/dissociation during ER stress. Despite this, both bZIP17 and bZIP28 have been shown to be active under different stresses such as heat, drought and salt stress in various plant species (Takahashi et al., 2012; Yang et al., 2013; Silva et al., 2015; Ramakrishna et al., 2018). However, functional differences between these two TFs have been observed. For instance, in *A. thaliana*, *bZIP28* is strongly induced by the ER-stressor DTT and TM (Tajima et al., 2008) whereas bZIP17 is more closely associated with salt stress responses (Liu et al., 2007). Interestingly, similar distinctions have been observed in rice: the orthologs of AtbZIP28 and AtbZIP17*,* respectively OsbZIP39 and OsbZIP60, respond in a same manner as

their Arabidopsis counterparts. Specifically, the transcript of *OsbZIP39* is induced by DTT and TM, but not by NaCl, suggesting that it may be a functional ortholog of AtbZIP28 rather than AtbZIP17 (Takahashi et al., 2012). Nevertheless, the precise functional differentiation between bZIP17 and bZIP28 remains not completely understood, reflecting both the conserved and lineage-specific regulatory complexity of UPR signaling across plant species.

Although the UPR is not yet fully understood, extensive studies in various plant species have provided valuable insights into its regulatory mechanisms. These studies have revealed differences in UPR activation and composition across species under various stress conditions. However, most research has primarily focused on few abiotic stresses like heat and salt, and even less studies examined biotic factors. Among these, the first evidence linking the UPR to plant immunity was obtained in *A. thaliana* and tobacco plants challenged with bacterial pathogens (Moreno et al., 2012; Arraño-Salinas et al., 2018) and viruses (Adhikari et al., 2025). More recently studies were expanded also to fungal or oomycetes infection (Qiang et al., 2021; Blanchard et al., 2025). In addition, *A. thaliana* is the most widely used model, limiting our understanding of UPR's role during pathogen attacks in different contexts.

In this study, we aimed to characterize the UPR in grapevine (*Vitis vinifera*), a worldwide economically important crop. Through a phylogenetic analysis we identified putative members of the two main UPR arms and analyzed the transcriptomic profiles of *VvIRE1, VvbZIP60, VvBIP3* and *VvbZIP17* in response to abiotic and biotic stresses. Our main results indicate that the well-known grapevine pathogens *Botrytis cinerea* and *Plasmopora viticola* induce UPR and that among other common stresses, copper sulfate treatment, heat and osmotic stress also trigger the UPR in *Vitis vinifera*.

2. Materials and methods

2.1. Plant materials

Vitis vinifera cv Marselan (*Vitis vinifera* cv. Cabernet Sauvignon x *Vitis vinifera* cv. Grenache noir) cell culture was obtained from callus initiated from petioles of grapevine leaves and cultivated in Nitsch-Nitsch medium (Nitsch and Nitsch, 1969) supplemented with 1 g/L casein hydrolysate, 400 µg/L 1-naphthaleneacetic acid and 40 µg/L 6-benzylaminopurine. The resulting cell suspension cultures were maintained under continuous light conditions (cool-white fluorescent lamps, 3350 lux) with constant agitation at 120 rpm and a temperature of 24°C. Sub-culturing was performed weekly by transferring 20 mL of the cell suspension into 100 mL of fresh medium. For experimental purposes, 7-day-old cultures were diluted to a 1:2 ratio with fresh medium one day prior to use.

V. vinifera cv Marselan herbaceous cuttings were grown in a greenhouse in control condition. The cuttings were grown individually in pots (8 cm × 8 cm × 8 cm) containing a 7:3 (v/v) mixture of peat and perlite at 23°C/15°C (day/night) with a 16-hour photoperiod. Plants were irrigated with a

balanced nutrient solution (N:P:K, 10-10-10; Plantin, France) and were utilized for experiments once they had developed 5 to 7 fully expanded leaves.

2.2. Phylogenetic analysis

Protein sequences of bZIP17, bZIP28, bZIP60, BIP and IRE1 were retrieved using tblastx searches, in which Arabidopsis family members were used as query sequences against protein sequences from plant species as detailed in Table S1. In addition, orthologous gene families were identified with OrthoFinder (v2.5.4). The bZIPs sequences were confirmed in different databases such as EnsemblPlants (https://plants.ensembl.org/index.html), NCBI (https://www.ncbi.nlm.nih.gov/) and UNIProt (https://www.uniprot.org/). Multiple full-length protein sequences alignment (ClustalW method) and a maximum-likelihood phylogenetic tree with 1000 bootstraps were used choosing the Maximum Likelihood method and JTT model (Jones et al., 1992). Alignment and phylogenetic analysis were performed with MEGA X software (Tamura et al., 2021).

2.3. Cell suspension treatments

Grapevine cell suspension was subjected to different abiotic stresses at the following final concentration: 2 mM dithiothreitol (DTT), 0.2 µg/mL tunicamycin (TM), 1% polyethylene glycol 8000 (PEG), 50 mM sodium chloride (NaCl), 0.1 mM of copper(II) sulfate (CuSO4), 0.1 mM of magnesium sulfate (MgSO4), 0.1 mM of copper(II) carbonate basic ($CuCO3 \cdot Cu(OH)_2$), 10 nM of XcFlg22 and 0.2 mg/mL of hexamer of chitin (CO6, GLU436), chitosan (CHITO, GLU426) and tetramer of chitin (CO4; GLU434). All treatments were diluted in water with the exception of the tunicamycin which was dissolved in dimethyl sulphoxide (DMSO). For heat and cold stress, 20 mL of grapevine cell suspension contained in a 50 mL flask were put in a water bath at 37˚C or put on a shaker plate in a cold room at 4˚C.

2.4. Pathogen infection

For *Botrytis cinerea* infection assays, leaf disks (1.9 cm diameter) from the upper third leaves of adult herbaceous cutting were transferred onto damp Whatmann paper in a plastic box and sprayed with a spore solution of $2.5*10^5$ spores/mL of *B. cinerea* or with quarter-strength PDB. The inoculated leaf discs were placed in a plastic box maintained at 100% humidity under a 10/14h day/night photoperiod at 20/18°C.

For *Plasmopora viticola* infection assays, the lower leaf surface of the first developed leaf was sprayed with a freshly prepared suspension of 10^4 sporangia/mL of *P. viticola*. Plants were maintained in 100% humidity overnight and later located in the greenhouse at 23°C/15°C (day/night) with a 16-hour photoperiod.

2.5. VvbZIP60 splicing assay

For gel-based bZIP60 splicing assay, 5 ng of ADNc were amplified by PCR with specific primers flanking the unconventional intron, VvbZIP60_F and VvbZIP60_R (Supplementary Table S2). PCR conditions for amplification were: initial denaturation: 3 min at 95°C; 45 s at 95°C, 30 s at 63°C and

30 s at 72°C during 35 cycles; final extension 5 min at 72°C. Subsequently, PCR products were resolved by gel electrophoresis on agarose (3% p/v) (Invitrogen) using TAE 0.5X as running buffer.

2.6. Real-time quantitative reverse transcription polymerase chain reaction (qRT-PCR)

Grapevine cell suspensions were treated and harvested 1 and 3 h after elicitors and abiotic stresses. For copper and sulfur treatments, samples were harvest 1 – 3 – 6 – 12 and 24 h after treatment. For pathogens infection test, leaf samples were harvest 5- and 7-days post *P. viticola* infection and after 24 – 48 and 72 hours post *B. cinerea* infection. Total plant RNAs were extracted using the SV Total RNA Isolation System kit (Promega) with DNAse treatment according to the supplier instructions for grapevine cell suspension and with the Plant/Fungi Total RNA Purification Kit (NORGEN) with some modifications for leaf disks. Reverse transcription (RT) was performed on 1 µg of total RNA using the High-Capacity cDNA Reverse Transcription kit (Applied Biosystems) for grapevine cell suspension and the SuperScript IV Reverse Transcriptase kit (Thermofisher) for leaf disks. Real-time qPCR was performed with 10 ng of complementary DNA (cDNA) thus generated, diluted in a total volume of 5 µL of GoTaq® qPCR Master Mix (Promega) for cell suspension and ABsolute QPCR Mix SYBR Green low ROX (Thermofisher) for grapevine leaves. cDNA from green and mature berries were kindly provided by Kelloniemi et al. Amplification of cDNA was carried out in a ViiA™ 7 Real-Time PCR system (Applied Biosystems) thermocycler according to the following program: 15 min denaturation and activation of DNA polymerase at 95°C followed by 40 cycles of 3 stages with 15 sec at 95°C (denaturation), 30 sec at 61°C (primer hybridization) and 30 sec at 72°C (amplification). A final step consisting of 15 sec at 95°C, 1 min at 61°C then increasing by 0.05°C per second until 95°C was finally performed to obtain the melting curves and thus confirm that the primers were specific of the target genes. Expression data were analyzed from the average of threshold cycle (CT) values taking into consideration the efficiency (E) of each reaction calculated by the LinRegPCR quantitative PCR data analysis program (Ruijter et al., 2009). The mean of the data resulting from the technical duplicates for each gene of interest was normalized on two reference genes: *VvVSP54 (Vitvi10g01135)*, *VvRPL18B (Vitvi05g00033)* for grapevine cell suspension and *VvVATP16 (Vitvi03g04022)* and *VvRPL18B (Vitvi05g00033)* for grapevine leaf (Terrier et al., 2005; Gamm et al., 2011). The sequences of primers used can be found in Supplementary Table S2.

2.7. Cell viability

Grapevine suspension cells were stained with Fluorescein Diacetate (FDA) probe diluted at 20 µg/mL in 0.26% acetone then observed under an epifluorescence microscope (λexc: 450-490 nm, λem: 515 nm (LP), magnification x20) (Leitz, model DMRB). For each treatment condition, at least 200 cells were counted twice.

2.8. Statistical analysis

For qPCR analysis, relative expression value from one treated or infection time-point was compared to the data of the control condition at the same time point using one-way ANOVA followed by a Tukey HSD Test. If necessary, data were converted in normal values through the "orderNorm transformation" (package : bestNormalize). Data were represented on the figures as Log2 of the fold change to the control condition.

3. Results

3.1. Grapevine conserves key components of both UPR arms

A previous study identified 55 members in the bZIP gene family in grapevine genome including VvbZIP24 (here renamed VvbZIP17) and VvbZIP41 (here renamed VvbZIP60) (Liu et al., 2014). To characterize potential bZIP transcription factors (TFs) and other actors involved in ER stress in *Vitis vinifera*, we conducted a phylogenetic analysis using reference sequences from *A. thaliana* and their relative orthologs in mammals and yeast. Concerning the bZIP TFs, we retrieved 28 protein sequences for bZIP60 and 50 protein sequences for bZIP17/28 (Table S1) from 19 tracheophyte species, including 12 dicotyledons (*Brassica napus, Brassica oleracea, Brassica rapa, Beta vulgaris, Camelina sativa, Glycine max, Lotus japonicus, Medicago truncatula, Nicotiana tabacum, Pisum sativum, Solanum lycopersicum and Vitis vinifera*), 7 monocotyledons (*Ananas comosus, Asparagus officinalis, Hordeum vulgare subsp. vulgare, Musa acuminata, Oryza sativa, Triticum aestivum and Zea mays*) and 3 bryophytes (*Marchantia paleacea, Marchantia polymorpha and Physcomitrium patens*). Protein alignments confirmed that all identified sequences corresponded to bZIP proteins, showing the highly conserved bZIP domain composed by the basic region and the leucin loop region (Table S1, Fig.S1A-B). The bZIP domain consists of two structural features located on a contiguous α-helix: a basic region of ∼16 amino acid residues containing a nuclear localization signal followed by an invariant N-x7-R/K motif that binds the DNA and a heptad repeat of leucines or other bulky hydrophobic amino acids (A/V/L/G/I/M/W/F/P) positioned exactly nine amino acids towards the C-terminus, creating an amphipathic helix (Jakoby et al., 2002; Zhang et al., 2016).

Contrary to numerous plants studied, which possess at least three bZIP involved in UPR signaling, only two grapevine sequences have been identified. The first protein sequence clustered within the dicotyledons-specific clade of bZIP60 not far from the reference sequence of *A. thaliana* as shown in the phylogenetic tree (Fig.1A). Both *A. thaliana* and *V. vinifera* bZIP60 coding sequences share the same mRNA kissing stem-loop structures with the consensus sequences (CTGCTG) containing the putative splicing sites (Fig.1B). Based on the known splicing pattern described in *A. thaliana*, we predicted a 23-nucleotides splicing which provokes a frameshift in the coding region, resulting in the synthesis of a new truncated protein. Structural prediction of the protein before and after splicing (Fig.1C) showed that splicing leads to the removal of the transmembrane domain (TMD) and the generation of an alternative open reading frame (ORF2), producing a new C-

terminal region that includes a nuclear localization signal (NLS). These changes are consistent with the activation of bZIP60 via splicing and its subsequent nuclear translocation, as described in *A. thaliana* (Nagashima et al., 2011). Additionally, the predicted 3D structure highlighted the conserved bZIP domain and transmembrane helix between *A. thaliana* and *V. vinifera* (Fig.1D), further supporting the identification of this sequence as VvbZIP60.

The second bZIP grapevine sequence grouped more closely to the bZIP17 sequences rather than within the clade including bZIP28 sequences, the latter resulted exclusively to the Brassicaceae family (Fig.2A). This finding suggests that in grapevine, as in most dicotyledons except for the Brassicaceae family, the only identified sequence is more closely related to bZIP17 than to bZIP28. Interestingly, within the monocotyledons' clade, two distinct subclades are observed, corresponding to the two putative rice bZIP17/28 sequences. Notably, OsbZIP39, here renamed OsbZIP17b, has been proposed to be the ortholog of Arabidopsis bZIP28 (Takahashi et al., 2012). In our analysis, OsbZIP17b does not cluster along with AtbZIP28, suggesting that monocotyledons may possess two or more homologs of bZIP17 rather than both bZIP17 and bZIP28. For instance, in maize, ZmbZIP34, here named ZmbZIP17b, was first considered as the ortholog of AtbZIP28 (Zhu et al., 2019), while in latter study, the same sequence have been referred as homolog of bZIP17, therefore naming it ZmbZIP17b (Ko and Brandizzi, 2021). In grapevine, the *in-silico* analysis of VvbZIP17 protein structure, showed a canonical basic leucine zipper (bZIP) domain near the N-terminus and a single transmembrane domain (TMD) positioned toward the C-terminus, consistent with its classification as a membrane-tethered transcription factor. The bZIP17 sequence alignment between *A. thaliana* and *V. vinifera* revealed also a conserved S1P motif cleavage (RRIL) in C-terminal and a S2P cleavage motif represented by a glycine within the hydrophobic TMD (Fig.2B, Table S1). Following proteolytic activation after ER stress, the N-terminal region is predicted to be cleaved, resulting in a truncated form of the protein retaining the bZIP domain but lacking the TMD (Fig.2B). Structural 3D alphafold prediction of the full-length VvbZIP17 superposed on AtbZIP17 protein structure highlighted the well-defined alpha-helical structures of the bZIP domain and the TMD (Fig.2C). We can observe the 5-heptad leucine/cysteine repeats all along the bZIP domain and the S2P cleavage site, represented by a glycine (G) in the TMD (Fig.2B-C). These predictions support a conserved mechanism of activation through regulated intramembrane proteolysis under ER stress conditions in both plant species.

To complete the characterization of the UPR actors in grapevine, we chose to conduct a phylogenetic analysis also for the chaperon proteins BIP and the ER-transmembrane protein IRE1. As for bZIP17, bZIP28 and bZIP60, we used the reference sequences of *A. thaliana*. The BIP coding genes are known to be upregulated by the UPR pathway. In particular, *BIP3* is the most highly upregulated by abiotic stresses or by ER stress agents (Tajima et al., 2008; Herath et al., 2020) compared to *BIP1* and *BIP2*. As for *A. thaliana* we identified three grapevine sequences for BIP, two of them clustered within the BIP1/2 clade and the other one within the BIP3 sequences (Fig.S2). We can also observe a third cluster separated from the BIP1/2 and BIP3 clades and

specifically for the monocotyledons. This group includes OsBIP4 and OsBIP5 which have been described to be involved in the ER stress response (Wakasa et al., 2012). Phylogenetic analysis of IRE1 sequences showed three distinct groups clustering each one with AtIRE1a, AtIRE1b and AtIRE1c respectively. The AtIRE1c clade did not root with the IRE1 sequences from human and yeast, in addition only Brassicaceae sequences were found, suggesting a specific and separate role in the Brassicaceae family for this protein. Two grapevine sequences were identified clustering each one with AtIRE1a and AtIRE1b respectively, suggesting two possible candidate orthologs for IRE1, here named VvIRE1a and VvIRE1b) (Fig.S3). In addition, IRE1 proteins alignment showed the identification of the ATP binding motif (VAVKR) and the Ser/Thr protein kinase motif (DLKPQN) highly conserved among the IRE1a/b groups (Table S1). These results allowed us to identify the main putative UPR actors in grapevine, VvbZIP60 and VvbZIP17 among with VvBIPs and VvIRE1s compared to other plant species.

3.2. ER stress induces the splicing of *VvbZIP60* in grapevine cell suspension

The unconventional splicing of *bZIP60* mRNA has been shown previously in *A. thaliana* and other plant species (Moreno et al., 2012; Wang et al., 2017; Kaur and Kaitheri Kandoth, 2021; Li et al., 2022). To examine whether Vitis vinifera bZIP60 mRNA could undergo the unconventional splicing, the expression pattern of the spliced form was analyzed in grapevine cell suspension after 1 and 3 h of DTT and TM treatments. To specifically detect the spliced form of *VvbZIP60* mRNA, we designed a set of primers that amplify both the spliced and unspliced versions. One of the reverse primers spans the two splice junction sites of the spliced *VvbZIP60* mRNA and can only anneal if the 23 bp have been removed during splicing, whereas the other anneals in the 23 bp of the unconventional intron (Fig.3A). RT-qPCR analysis revealed that the expression of *VvbZIP60* spliced form was strongly induced upon DTT and TM treatment both at 1 and 3 h post treatment (hpt) (F-S primers, Fig.3A-B) and not in water or DMSO control, respectively. A slight difference was highlighted at 1 hpt where the TM treatment was less intense compared to DTT at the same time point. DTT and TM treatments also had an effect on the expression of the *VvbZIP60 unspliced* form (Fig.S4). Notably, DTT treatment provoked a decrease in unspliced mRNA amount at 1 hpt, while at 3 hpt it starts to increase (Fig.S4). To further confirm this event in grapevine, we checked the splicing of *VvbZIP60* in the same treated samples using the well-established PCR-based splicing assay, using a set of primers which could amplify the surrounding region of the splicing site (F-R primers, Fig. 3A). Using *VvVPS54* transcript as a loading control, a single band of 248 pb corresponding to the unspliced form was observed in the control H_2O- and DMSO-treated grapevine cell suspensions (Fig. 3C). Interestingly, a second band of 225 pb, corresponding to the spliced forms of *VvbZIP60*, was detected only in samples treated with DTT or TM (Fig.3C). A third band is also visible at around 250 pb, probably formed by the hybridization of bZIP60u and bZIP60s products during the PCR amplification. Such an hybrid band has been previously observed and documented in RT-PCR analysis of *XBP-1* and *bZIP60* in Human and Arabidopsis, respectively (Shang and Lehrman, 2004; Moreno et al., 2012). These two independent methods

confirm that *VvbZIP60* is regulated in a similar manner to other plant *bZIP60* and that the unconventional splicing happens at the predicted sites.

3.3. Heat and osmotic stress trigger UPR pathways in grapevine cell suspension

Previous results have confirmed the involvement of the UPR during different abiotic stresses such as heat, salt and drought (Liu et al., 2007; Valente et al., 2009; Deng et al., 2011). It is well known that grapevine faces adverse environmental conditions all along its development, coping for example with extreme temperatures. In order to identify which environmental stress could promote the activation of the UPR in grapevine, a series of abiotic stresses including salt stress (NaCl), osmotic stress (PEG), heat stress (37˚C) and cold stress (4˚C) were applied for 1 and 3 h to grapevine cell suspension. In addition, DTT, which is a reducing agent that inhibits the proper folding of disulfide bonds through the disturbance of the redox environment (Braakman et al., 1992), was also used as internal positive control. We chose to focus on the transcript response of five UPR genes: *VvbZIP60* unspliced and spliced forms, *VvbZIP17*, *VvBIP3*, *VvIRE1a* and *VvIRE1b*. As expected, DTT treatment strongly induced the splicing of *VvbZIP60* and the expression of *VvBIP3* at both time points (Fig. 4). Surprisingly, the expression of *VvbZIP17* and both *VvIRE1s* did not increase after the same treatment (Fig. 4). Salt stress (NaCl) among with cold temperature (4°C) did not upregulate the UPR genes at 1 and 3 hpt (Fig. 4). On the other hand, both high temperature (37°C) and PEG-induced osmotic stress strongly upregulated the expression of UPR genes at least at one time point, except for *VvIRE1a* and *VvIRE1b* only for PEG treatment (Fig. 4). In particular, heat stress (37°C) markedly induced the splicing of *VvbZIP60*, with the strongest response observed at 1 hpt and the expression of *VvbZIP17, VvBIP3* being significantlyinduced at 1 and 3 hpt. Interestingly, only *VvIRE1b* was upregulated at 3 hpt. In contrast, PEG-induced osmotic stress triggered a differential effect on the two UPR arms, with a stronger induction of *BIP3* and *bZIP60* expression at both time points, while *VvbZIP17* expression increased only at the later time point (Fig.4). These results suggest that the UPR is effectively activated during abiotic stresses, with differences in the timing of induction and the specific arm of the pathway involved.

3.4. Copper sulfate induces UPR pathways in grapevine cell suspension

In viticulture, copper (Cu) is widely used as the active ingredient in many fungicide mixtures, especially in organic farming. Copper-based fungicides like Bordeaux mixture have been used massively in viticulture notably against *P. viticola*. Unfortunately, their excessive use has led to the accumulation of copper in vineyard soils, raising environmental concerns. Excess copper can cause plant toxicity and pose risks to aquatic and soil organisms, making its long-term use controversial (Juang et al., 2012; Martins et al., 2015). While the increasing evidence of copper toxicity for soil and microorganisms, little is known about its effect on the ER stress and its effectiveness on protein folding in grapevine plants. A recent study, explored this hypothesis on *A. thaliana* seedling showing an increased stress in the ER after different heavy metal treatments (Demircan et al., 2024). To assess the effect of copper treatment on protein folding and UPR

activation, we decided to treat grapevine cell suspension with 0.1 mM copper sulfate ($CuSO_4$), magnesium sulfate ($MgSO_4$), and copper carbonate ($CuCO_3$) and check the transcriptomic response of the main UPR genes. Copper, whether formulated with sulfur as in the Bordeaux mixture or with carbonate, induced the expression of the unspliced form of *VvbZIP60, VvbZIP17* and *VvBIP3* within 3 hpt (Fig. 5). $MgSO_4$ showed no effect on all tested UPR genes at 1 and 3 hpt (Fig.5). Only *VvIRE1b* was specifically induced by $CuSO_4$ at 1 hpt (Fig. 5) whereas the spliced form of *VvbZIP60* was significantly upregulated by $CuSO_4$ at 3 hpt (Fig. 5). This trend was further confirmed in a longer kinetic analysis, where both copper treatments induced the expression of UPR genes also at later time points (Fig.S5). On the whole, these results confirm that copper, in addition to its toxic effects on soil, can also induce ER stress in plant and consequently activate the UPR. Furthermore, sulfate, commonly used alongside copper in fungicide formulations, did not induce UPR responsive genes, suggesting that it does not interfere with ER function when it is associated with magnesium at this concentration.

3.5. *VvbZIP17* and *VvbZIP60* gene expression are upregulated by chitosan

In previous work, bacterial microbe-associated molecular patterns (MAMPs) were shown to induce the expression of UPR genes (Arraño-Salinas et al., 2018; Chakraborty et al., 2020). Grapevine mainly faces several fungal pathogens and chitinaceous molecules derived from these interactions are known to trigger grapevine immunity (Brulé et al., 2019; Brulé et al. 2024). To assess whether UPR is triggered by MAMPs, we treated grapevine cell suspensions with three different chitin oligomers (COs) of different degree of polymerization (DP): DP4 (CO4), DP6 (CO6) and chitosan DP6 (CHITO) and the most active epitope of the bacterial flagellin (XcFlg22) (Trdá et al., 2014). We observed that none of these MAMP induced the UPR at 1 and 3 hpt except for chitosan, which significantly increased the expression of all UPR genes at 3 hpt, except *VvBIP3* (Fig.6). Interestingly, chitosan was also the only MAMP to exhibit toxicity in cell suspensions: between 3 and 24 hpt, the cell viability decreased by up to 50% compared to the control and other treatments (Fig.S6). These results suggest a possible link between UPR and chitosan-induced cell death.

3.6. The grapevine pathogens *B. cinerea* and *P. viticola* trigger UPR pathways

Increased accumulation of UPR gene transcripts such as *bZIP60* and *bZIP17* have been reported during several plant-pathogen interactions (Xu et al., 2019; Blanchard et al., 2025). To investigate if grapevine pathogens influence the activation of the UPR, we inoculated grapevine cuttings grown in greenhouse with *P. viticola*, the causal agent of downy mildew and *B. cinerea* which is responsible for the grey mold disease. *P. viticola* was applied directly to the leaves of whole grapevine cuttings (Fig. S7A), whereas *B. cinerea* was inoculated on leaf disks (Fig.S7C). Infection was confirmed by quantifying transcript levels of grapevine immune genes, such as acidic chitinase (*CHIT4C*) and stilbene synthase (*STS*), using RT-qPCR at various time points. Both pathogens strongly induced the defense-related genes at all time points (Fig.S7B, D). At 5 days post inoculation (dpi), *P. viticola* triggered the splicing of *VvbZIP60* and increased the expression level of *VvbZIP17*, *VvBIP3* and *VvIRE1b* (Fig.7A). At 7 dpi, only the *VvbZIP60* spliced form and

VvIRE1b were significantly upregulated (Fig.7A). At 5 dpi, *P. viticola* did not reach full sporulation since mycelium was not visible, whereas at 7 dpi the abaxial side of the leaves was fully colonized by the oomycete (Fig.S7A). These results suggest that ER stress might be an early response during *P. viticola* infection. Similarly, *B. cinerea* also induced the activation of all UPR genes in grapevine leaves at 24, 48 or 72 hpi with a strong induction of the *VvbZIP60* splicing was strongly induced at all time points (Fig. 7B). *VvbZIP17* and *VvIRE1b* showed an increased expression only at 48 and 72 h post inoculation (hpi), while *VvBIP3* was significantly induced only at 72 hpi (Fig.7B). *B. cinerea* is a necrotrophic pathogen that causes substantial damages mainly on grapevine berries. Green berries (GB), or berries that are close to the veraison stage, show basal resistance to this pathogen (Deytieux-Belleau et al., 2009; Kelloniemi et al., 2015). On the other hand, mature berries (MB) are more susceptible and are often infected by *B. cinerea*, impacting the phenolic and organoleptic properties of wines (Kretschmer et al., 2007; Ky et al., 2012). We thus decided to analyze the expression of UPR genes in GB and MB infected by *B. cinerea* after 24 and 48 hpi. On green berries, UPR genes did not seem to be induced with the exception of *VvbZIP17* which showed an increased expression at 24 hpi (Fig.7C), on mature berries *B. cinerea* infection induced the upregulation of Vv*bZIP60* spliced, Vv*bZIP17* and Vv*BiP3* (Fig.7D). Together, these results show a clear involvement of both UPR arms during the interaction between *V. vinifera* and both *P. viticola* and *B. cinerea.*

4. Discussion

An increasing number of studies have demonstrated a strong link between the plant's surrounding environment, including both abiotic factors and microorganisms' interaction, and the activation of the UPR (Adhikari et al., 2025; Liu et al., 2025; Ko and Brandizzi, 2024). In this study, we identified the grapevine ortholog of bZIP60, designated as VvbZIP60 and demonstrated that its transcript undergoes unconventional splicing in response to ER stress induced by DTT and TM (Fig. 3). Notably, VvbZIP60 harbors two conserved kissing stem-loop structures in its mRNA, essential for IRE1-mediated splicing. In other plant species, splicing at these sites leads to a frameshift, generating a new protein lacking the transmembrane domain (Moreno et al., 2012; Kaur and Kaitheri Kandoth, 2021). We also identified two putative grapevine orthologs of the ER-transmembrane sensor IRE1, VvIRE1a and VvIRE1b. Interestingly, *VvIRE1b* consistently exhibited higher expression levels than *VvIRE1a* under most of the stress conditions analyzed. Notably, during infections with both *P. viticola* and *B. cinerea*, *VvIRE1b* showed a significantly stronger transcriptional induction compared to its counterpart *VvIRE1a* (Fig.7A-B), suggesting a potentially more prominent role in initiating the UPR during grapevine immunity. Interestingly, in *A. thaliana*, neither *IRE1a* nor *IRE1b* is transcriptionally induced upon *B. cinerea* infection (Blanchard et al., 2025), although IRE1b plays a dominant role in *bZIP60* splicing (Deng et al., 2011; Moreno et al., 2012). In addition, IRE1b's RNase activity is required for ER stress-induced autophagy via RIDD, independently of bZIP60 (Bao et al., 2018). Given that autophagy contributes to plant defense

against necrotrophs like *B. cinerea* (Lai et al., 2011), VvIRE1b may integrate both bZIP60 splicing and RIDD-autophagy pathways in grapevine stress responses. Further studies are needed to clarify the functional roles of both IRE1 isoforms. The second major arm of the UPR in plants is defined by the bZIP17/28 signaling module. Interestingly, our phylogenetic analysis revealed the presence of a single grapevine bZIP sequence clustering with bZIP17, while no grapevine sequence grouped with the bZIP28 clade. In the dicotyledons, bZIP28 orthologs were found to be exclusive members of the Brassicaceae. This arm of the pathway may be therefore lineage-specific and absent in non-Brassicaceae species such as *Vitis vinifera*. This finding highlights possible evolutionary divergence in UPR signalling components among dicotyledonous species and raises questions about how UPR is regulated in species lacking the bZIP28 arm.

The UPR is known to be induced by different abiotic and biotic stresses. Here, we observed a significant induction of both UPR arms, under a variety of stress conditions. Among the abiotic factors tested in this study, heat and osmotic stress were the stronger ER-stressors with a high induction of *VvbZIP60* splicing, *VvBiP3* and *VvbZIP17* transcript levels. Heat stress is a well-known ER-stress inducer which provokes the splicing of *bZIP60* in different plant species such as *A. thaliana*, tomato and rice (Deng et al., 2011; Takahashi et al., 2012; Kaur and Kaitheri Kandoth, 2021). On the other hand bZIP17 was only described to play important roles in maintaining fertility under heat stress conditions in *Arabidopsis* (Gao et al., 2022). A transcriptomic analysis revealed that *VvbZIP17* was upregulated in responses to drought stress (Liu et al., 2014) but no previous studies focused on the PEG-induced osmotic stress. Interestingly, in *A. thaliana*, bZIP17 was found to be more involved in the response to salt (Liu et al., 2007). In grapevine cell suspension, NaCl treatment did not induce the UPR. Grapevine is relatively tolerant to salt stress, likely due to its adaptation to drought-prone environments. In a recent study, a transcriptome analysis of all *bZIP* TFs was conducted in grapevine to analysis their response to salt stress. Several *bZIPs* were upregulated under salt stress however neither *VvbZIP17* nor *VvbZIP60* showed significant changes in expression (Guan et al., 2018; Çakır Aydemir et al., 2020). These results highlight the complexity of the UPR and suggest that its activation may vary between plant species.

One interesting result obtained in this study is that copper treatment induces the UPR in grapevine cells. This finding is consistent with previous studies in Arabidopsis seedlings, where elevated copper levels impact seedling growth and also activated the UPR (Demircan et al., 2024). Notably, elevated copper levels are often found in vineyard soils and have been shown to affect root development (Juang et al., 2019). These observations suggest that copper stress, in addition to its known effects on oxidative damage and metal homeostasis, may impair protein folding in the ER, thereby triggering ER stress and impacting plant development. While the UPR is commonly associated with various abiotic stresses, copper-induced activation highlights a potentially underexplored aspect of copper toxicity. Further studies are therefore needed to determine

whether copper directly disrupts ER-resident proteins or causes secondary oxidative effects that lead to protein misfolding and ER stress. Notably, copper exposure provoke an accumulation of ROS and oxidative damage on *A. thaliana* roots and shoots (Wang et al., 2022). In addition, oxidative stress, in particular, increasing level of singlet oxygen ($^1O_2$), has also been demonstrated to trigger ER stress and induce the UPR response, confirming the interplay between ROS and UPR (Ozgur et al., 2018; Beaugelin et al., 2020)

The primary recognition of microorganisms involves the perception of highly conserved molecular signatures, also known as MAMPs. MAMPs are found in many types of microorganisms, including bacteria, fungi, viruses and protozoa and tend to be highly conserved, meaning that they are structurally similar across different species of microbes (Newman et al., 2013). A study carried out in *A. thaliana* seedlings, showed that the UPR genes, notably *IRE1a* and *IRE1b*, were induced after treatment with the flagellin-derived peptide flg22 and elongation factor Tu-derived peptide elf18, suggesting an impact of these MAMPs on the ER-homeostasis (Chakraborty et al., 2020). Here we decided to test several MAMPs, including flg22 and chitinous molecules such as chitin at different DPs and chitosan. Surprisingly, only chitosan could induce the UPR, particularly the transcription of *VvbZIP17* (Fig.6). Chitosan is a deacetylated derivative of chitin and is known to be a potent elicitor of plant immunity. In grapevine it exhibits antimicrobial properties against *B. cinerea*, *P. viticola* and Esca disease agents (Mian et al., 2023; Martín et al., 2023; Brulé et al., 2024). Chitosan-triggered immunity is associated to a set of cellular and molecular changes including cell wall lignification and callose deposition, ROS production, ion fluxes associated with the plasma membrane depolarization, MAPK activation, phytoalexin and defense-responsive proteins biosynthesis (El Hadrami et al., 2010; Narula et al., 2020; Brulé et al., 2024). Interestingly, it has been demonstrated that ROS production affects the ER stress response in plants, acting as secondary messengers (Ozgur et al., 2018) and that UPR is also involved in lignin deposition (Nakamura et al., 2022). In addition, chitosan has been shown to trigger cell death in grapevine suspension cells (this study) and in soybean cells, where it occurs via activation of a caspase-3-like protease (Zuppini et al., 2004). This protease activity is well-known to be involved in ER stress-induced plant cell death (Cai et al., 2014). These findings suggest that chitosan-induced cell death may be linked to UPR signaling through protease activity, although further studies are needed to confirm this connection.

We showed in this study that *P. viticola* and *B. cinerea* upregulate all UPR genes with the exception of *VvIRE1a* in grapevine leaves. Interestingly, during *B. cinerea* infection, we observed a different time-dependent induction of the two arms of the UPR, suggesting that the necrotrophic pathogen *B. cinerea* primarily engages the bZIP60 arm of the UPR, while bZIP17 plays a more restricted role in the response. We also obtained similar results on grapevine mature berries infected by *B. cinerea*. Interestingly, the UPR activation coincided with a marked accumulation of

jasmonate-isoleucine (JA-Ile) in mature berries (Kelloniemi et al., 2015). Previous studies in *Nicotiana attenuata* have shown that exogenous methyl jasmonate (MeJA) application strongly induce *BIP3* and splicing of *bZIP60* (Xu et al., 2019). These findings suggest a potential link between JA signaling and UPR activation during necrotrophic fungal infection in grapevine. While *VvbZIP17* is upregulated in grapevine mature berries, we also found a strong upregulation of this gene in green berries. Interestingly, in resistant green berries a strong H_2O_2 production is detected which is associated with the expression of *VvRbohD* and linked to a modification of the redox status while in mature berries the Gene Ontology term "cell death" is enriched and cell death is observable under the microscope (Kelloniemi et al., 2015). This redox stress could be responsible for the induction of bZIP17 expression in green berries, whereas in mature infected berries, bZIP17 seems to be more associated with the induction of cell death. However, further studies are needed to understand if the UPR, and notably *VvbZIP17*, is induced up- or downstream of these different events. To better understand the specific role of each UPR component, more in-depth functional genomic studies will be required, including CRISPR/Cas9-mediated knockouts in grapevine (Villette et al., 2024) and complementation of *Arabidopsis* mutants with grapevine genes. Recent findings show that the simple mutant *bzip17* is more resistant to *B. cinerea* infection, suggesting that bZIP17 may also act as a negative regulator of defense (Blanchard et al., 2025). Since VvbZIP17 is expressed in all grapevine organs (Liu et al., 2014), it is possible that it may act differently in berries and leaves and in different plant species.

Conclusion

All together, these findings suggest that the IRE1/bZIP60 and bZIP17 arms of the UPR are not only structurally conserved in grapevine but also transcriptionally regulated by a broad range of abiotic and biotic stresses. Notably, their expression patterns are modulated in an organ- and time-specific manner, highlighting a complex and finely tuned regulatory mechanism. These observations underscore the potential role of UPR signaling in grapevine stress adaptation and defense. To fully elucidate the functional relevance of these pathways, further studies integrating proteomic and Knock-out by genome editing technology will be essential, particularly to define their contribution to stress resilience and tolerance to pathogen infections, with an emphasis on the link between ROS production and UPR.

Appendix A. Supplementary data

Fig. S1. bZIP domain sequences alignment. (A) bZIP60 domain sequences and **(B)** bZIP17/28 domain sequences alignment. The bZIP domain consists of two structural features: a basic region of ~16 amino acid residues containing a nuclear localization signal followed by an invariant N-x7-R motif that binds the DNA and a heptad repeat of leucines or other bulky hydrophobic amino acids (A/V/L/G/I/M/W/F/P) positioned exactly nine amino acids towards the C-terminus.

Fig. S2. Phylogenetic analysis of BIP family. Phylogenetic tree of bryophyte in orange, basal angiosperms, monocotyledons (yellow) and dicotyledons (green) represented in different colors. The phylogenetic tree is rooted with human HsGRP78 and the yeast ScKAR2 sequences. Red asterisk indicated *Vitis vinifera* sequences. The phylogenetic tree was constructed using MEGA11 software with the maximum-likelihood method and a bootstrap consensus of 1,000 bootstraps

Fig. S3. Phylogenetic analysis of IRE family. Phylogenetic tree of bryophyte in orange, basal angiosperms, monocotyledons (yellow) and dicotyledons (green) represented in different colors. The phylogenetic tree is rooted with human HsIRE1a, HsIRE1b and yeast ScIRE sequences. Red asterisk indicated *Vitis vinifera* sequences. The phylogenetic tree was constructed using MEGA11 software with the maximum-likelihood method and a bootstrap consensus of 1,000 bootstraps

Fig. S4. Expression of *VvbZIP60 unspliced* after DTT and TM treatment. Log2-fold change values of *VvbZIP60 unspliced* form measured by qRT-PCR 1 and 3 hours after 2 mM dithiothreitol (DTT), 0.2 µg/ml tunicamycin (TM) treatments and their respective negative control water and dimethyl sulfoxide (DMSO). Barplots represent the distribution of four independent biological repeats (n=4). Means of technical duplicates (efficiency-weighted Cq(w) values) were normalized using mean Cq(w) data of two housekeeping genes (*VvVSP54 and VvRPL18B*) before being analyzed. Asterisks indicate statistically significant differences between negative controls and the relative treatments using a ANOVA test followed by a TukeyHSD post doc test, ($P< 0.05$).

Fig. S5. Copper treatments triggers both UPR pathways. Log2-fold change values of *VvbZIP60 unspliced* and *spliced* form, *VvbZIP17*, *VvBIP3, VvIRE1a* and *VvIRE1b* measured by qRT-PCR 1 - 3 - 6 - 12 - 24 hours after 0,1 mM copper(II) sulfate ($CuSO_4$), magnesium sulfate ($MgSO_4$), and copper(II) carbonate ($CuCO_3$). Data represent the Log2 of the Fold change of four independent biological repeats (n=4) normalized on the negative (dot line). Means of technical duplicates (efficiency-weighted Cq(w) values) were normalized using mean Cq(w) data of two housekeeping genes (*VvVSP54* and *VvRPL18B*) before being analyzed. Data were converted in normal values through the “orderNorm transformation” (package : bestNormalize). Asterisks indicate statistically significant differences between negative control and the relative treatments using a ANOVA test followed by a TukeyHSD post doc test, ($P< 0.05$).

Fig. S6. Chitosan induces dell death on grapevine suspension cell. Cell counting was performed 3 and 24 hours after 2 mM dithiothreitol (DTT), 0.2 µg/ml tunicamycin (TM), 0,2 mg/ml short-chitooligosaccharide DP4 (CO4), chitin DP6 (CO6), chitosan DP6 (CHITO) treatments and their respective negative control water and dimethyl sulfoxide (DMSO). Cells were stained with FDA probe then observed under an epifluorescence microscope (λexc: 450-490 nm, λem: 515 nm (LP), magnification x20) (Leitz, model DMRB). Values are mean ± SD of three independent replicates among which was counted at least 500 cells. Results are statistically equivalent to the corresponding negative control according to pairwise prop-tests with Holm correction to inflate the p-values. Each treatment has been studied individually. Statistical analysis was performed using

one-way ANOVA followed by Tukey's post-hoc test to compare treatments within each time point. Different letters indicate statistically significant differences between groups ($p < 0.05$).

Fig. S7. *P. viticola* and *B. cinerea* trigger defence-gene expression. **(B-D)** Log2-fold change values of defence-gene *VvCHIT4C and VvSTS1.2* measured by qRT-PCR 5-7 days post infection with *P. viticola* and 24-48-72 hours post infection with *B. cinerea* and their respective negative control water set at 0. Barplots represent the distribution of six and four independent biological repeats (n=6/n=4) respectively. Means of technical duplicates (efficiency-weighted Cq(w) values) were normalized using mean Cq(w) data of two housekeeping genes (*VvVATP16* and *VvEF1a*) before being analyzed. Data were converted in normal values through the "orderNorm transformation" (package : bestNormalize). Asterisks indicate statistically significant differences between negative controls and the relative treatments using a ANOVA test followed by a TukeyHSD post doc test, ($P< 0.05$). **(A-C)** Photos of infected leaves and leaf disks at different time points with *P. viticola* and *B. cinerea* respectively,

Table S1. bZIPs sequence and alignment

Table S2. Primers used in this study

Acknowledgements

We acknowledge Dr. Benoit Darblade (Elicityl, Crolles, France) for the CO6, CO4 and chitosan oligomers.

Author contributions

TM performed most of the experiments, analyzed the data, and wrote the original draft. CB executed part of the RTqPCR. EP created the graphical abstract. KP was responsible of grapevine cutting production. AK was responsible of grapevine cell suspension development. AM performed the analysis in OrthoFinder. AH partially contributed to RNA extraction. BP and MG oversaw the project and conducted the critical review and revision of the manuscript. All authors contributed to the article and approved the submitted version.

Conflict of interest

The authors declare no potential conflict of interest.

Funding

This work has been financially supported by ANER-Région Bourgogne Franche-Comté grant UPRInFoVigne and Ministère de l'Enseignement Supérieur et de la Recherche for the funding of Tania Marzari, Emma Poilvert, Alix Martinez, and Aurélien Henry's PhD grants (MESRI).

Data availability

All data supporting the findings of this study are available within the paper and its supporting information are published online, the materials of this study are available from the corresponding author upon reasonable request.

Declaration of generative AI and AI-assisted technologies in the writing process.

During the preparation of this work the authors used “chatGPT” in the writing process to improve the readability and language of the manuscript. After using this tool, the authors reviewed and edited the content as needed and take full responsibility for the content of the published article.

References

Adhikari, B., Verchot, J., Brandizzi, F., Ko, D.K., 2025. ER stress and viral defense: Advances and future perspectives on plant unfolded protein response in pathogenesis. Journal of Biological Chemistry 301, 108354. https://doi.org/10.1016/j.jbc.2025.108354

Arraño-Salinas, P., Domínguez-Figueroa, J., Herrera-Vásquez, A., Zavala, D., Medina, J., Vicente-Carbajosa, J., Meneses, C., Canessa, P., Campos-Vargas, R., Moreno, A.A., Blanco-Herrera, F., 2018. WRKY7, -11 and -17 transcription factors are modulators of the bZIP28 branch of the unfolded protein response during PAMP-triggered immunity in Arabidopsis thaliana. Plant Science 277, 242–250. https://doi.org/10.1016/j.plantsci.2018.09.019

Bao, Y., Pu, Y., Yu, X., Gregory, B.D., Srivastava, R., Howell, S.H., Bassham, D.C., 2018. IRE1B degrades RNAs encoding proteins that interfere with the induction of autophagy by ER stress in *Arabidopsis thaliana*. Autophagy 14, 1562–1573. https://doi.org/10.1080/15548627.2018.1462426

Beaugelin, I., Chevalier, A., D’Alessandro, S., Ksas, B., Havaux, M., 2020. Endoplasmic reticulum-mediated unfolded protein response is an integral part of singlet oxygen signalling in plants. The Plant Journal 102, 1266–1280. https://doi.org/10.1111/tpj.14700

Bertolotti, A., Zhang, Y., Hendershot, L.M., Harding, H.P., Ron, D., 2000. Dynamic interaction of BiP and ER stress transducers in the unfolded-protein response. Nat Cell Biol 2, 326–332. https://doi.org/10.1038/35014014

Blanchard, C., Aimé, S., Ducloy, A., Hichami, S., Azzopardi, M., Cacas, J.-L., Lamotte, O., 2025. The IRE1-bZIP60 branch of Unfolded Protein Response is required for *Arabidopsis* immune response to *Botrytis cinerea*. Journal of Experimental Botany eraf244. https://doi.org/10.1093/jxb/eraf244

Braakman, I., Helenius, J., Helenius, A., 1992. Manipulating disulfide bond formation and protein folding in the endoplasmic reticulum. The EMBO Journal 11, 1717–1722. https://doi.org/10.1002/j.1460-2075.1992.tb05223.x

Brulé, D., Héloir, M.-C., Roudaire, T., Villette, J., Bonnet, S., Pascal, Y., Darblade, B., Crozier, P., Hugueney, P., Coma, V., Poinssot, B., 2024. Increasing vineyard sustainability: innovating a targeted chitosan-derived biocontrol solution to induce grapevine resistance against downy and powdery mildews. Front. Plant Sci. 15. https://doi.org/10.3389/fpls.2024.1360254

Brulé, D., Villano, C., Davies, L.J., Trdá, L., Claverie, J., Héloir, M., Chiltz, A., Adrian, M., Darblade, B., Tornero, P., Stransfeld, L., Boutrot, F., Zipfel, C., Dry, I.B., Poinssot, B., 2019. The grapevine (*Vitis vinifera*) LysM receptor kinases Vv LYK 1-1 and Vv LYK 1-2 mediate chitooligosaccharide-triggered immunity. Plant Biotechnol J 17, 812–825. https://doi.org/10.1111/pbi.13017

Cai, Y.-M., Yu, J., Gallois, P., 2014. Endoplasmic reticulum stress-induced PCD and caspase-like activities involved. Front. Plant Sci. 5. https://doi.org/10.3389/fpls.2014.00041

Çakır Aydemir, B., Yüksel Özmen, C., Kibar, U., Mutaf, F., Büyük, P.B., Bakır, M., Ergül, A., 2020. Salt stress induces endoplasmic reticulum stress-responsive genes in a grapevine rootstock. PLoS ONE 15, e0236424. https://doi.org/10.1371/journal.pone.0236424

Chakraborty, R., Uddin, S., Macoy, D.M., Park, S.O., Van Anh, D.T., Ryu, G.R., Kim, Y.H., Lee, J.-Y., Cha, J.-Y., Kim, W.-Y., Lee, S.Y., Kim, M.G., 2020. Inositol-requiring enzyme 1 (IRE1) plays for AvrRpt2-triggered immunity and RIN4 cleavage in Arabidopsis under endoplasmic reticulum (ER) stress. Plant Physiology and Biochemistry 156, 105–114. https://doi.org/10.1016/j.plaphy.2020.09.002

Chen, X., Shen, J., Prywes, R., 2002. The Luminal Domain of ATF6 Senses Endoplasmic Reticulum (ER) Stress and Causes Translocation of ATF6 from the ER to the Golgi. Journal of Biological Chemistry 277, 13045–13052. https://doi.org/10.1074/jbc.M110636200

Demircan, N., Ozgur, R., Turkan, I., Uzilday, B., 2024. Heavy metal toxicity leads to accumulation of insoluble proteins and induces endoplasmic reticulum stress–specific unfolded protein response in Arabidopsis thaliana. Environ Sci Pollut Res 31, 53206–53218. https://doi.org/10.1007/s11356-024-34780-y

Deng, Y., Humbert, S., Liu, J.-X., Srivastava, R., Rothstein, S.J., Howell, S.H., 2011. Heat induces the splicing by IRE1 of a mRNA encoding a transcription factor involved in the unfolded protein response in Arabidopsis. Proc. Natl. Acad. Sci. U.S.A. 108, 7247–7252. https://doi.org/10.1073/pnas.1102117108

Deytieux-Belleau, C., Geny, L., Roudet, J., Mayet, V., Donèche, B., Fermaud, M., 2009. Grape berry skin features related to ontogenic resistance to Botrytis cinerea. Eur J Plant Pathol 125, 551–563. https://doi.org/10.1007/s10658-009-9503-6

El Hadrami, A., Adam, L.R., El Hadrami, I., Daayf, F., 2010. Chitosan in Plant Protection. Marine Drugs 8, 968–987. https://doi.org/10.3390/md8040968

Gamm, M., Héloir, M.-C., Kelloniemi, J., Poinssot, B., Wendehenne, D., Adrian, M., 2011. Identification of reference genes suitable for qRT-PCR in grapevine and application for the study of the expression of genes involved in pterostilbene synthesis. Mol Genet Genomics 285, 273–285. https://doi.org/10.1007/s00438-011-0607-2

Gao, J., Wang, M.-J., Wang, J.-J., Lu, H.-P., Liu, J.-X., 2022. bZIP17 regulates heat stress tolerance at reproductive stage in Arabidopsis. aBIOTECH 3, 1–11. https://doi.org/10.1007/s42994-021-00062-1

Gardner, B.M., Walter, P., 2011. Unfolded Proteins Are Ire1-Activating Ligands That Directly Induce the Unfolded Protein Response. Science 333, 1891–1894. https://doi.org/10.1126/science.1209126

Gayral, M., Arias Gaguancela, O., Vasquez, E., Herath, V., Flores, F.J., Dickman, M.B., Verchot, J., 2020. Multiple ER-to-nucleus stress signaling pathways are activated during *Plantago asiatica mosaic virus* and *Turnip mosaic virus* infection in *Arabidopsis thaliana*. Plant J 103, 1233–1245. https://doi.org/10.1111/tpj.14798

Guan, L., Haider, M.S., Khan, N., Nasim, M., Jiu, S., Fiaz, M., Zhu, X., Zhang, K., Fang, J., 2018. Transcriptome Sequence Analysis Elaborates a Complex Defensive Mechanism of Grapevine (Vitis vinifera L.) in Response to Salt Stress. IJMS 19, 4019. https://doi.org/10.3390/ijms19124019

Hayashi, S., Wakasa, Y., Takahashi, H., Kawakatsu, T., Takaiwa, F., 2012. Signal transduction by IRE1-mediated splicing of *bZIP50* and other stress sensors in the endoplasmic reticulum stress response of rice. The Plant Journal 69, 946–956. https://doi.org/10.1111/j.1365-313X.2011.04844.x

Herath, V., Gayral, M., Adhikari, N., Miller, R., Verchot, J., 2020. Genome-wide identification and characterization of Solanum tuberosum BiP genes reveal the role of the promoter architecture in BiP gene diversity. Sci Rep 10, 11327. https://doi.org/10.1038/s41598-020-68407-2

Hollien, J., 2013. Evolution of the unfolded protein response. Biochimica et Biophysica Acta (BBA) - Molecular Cell Research 1833, 2458–2463. https://doi.org/10.1016/j.bbamcr.2013.01.016

Howell, S.H., 2013. Endoplasmic Reticulum Stress Responses in Plants. Annu. Rev. Plant Biol. 64, 477–499. https://doi.org/10.1146/annurev-arplant-050312-120053

Iwata, Y., Koizumi, N., 2005. Unfolded protein response followed by induction of cell death in cultured tobacco cells treated with tunicamycin. Planta 220, 804–807. https://doi.org/10.1007/s00425-004-1479-z

Jakoby, M., Weisshaar, B., Dröge-Laser, W., Vicente-Carbajosa, J., Tiedemann, J., Kroj, T., Parcy, F., 2002. bZIP transcription factors in Arabidopsis. Trends in Plant Science 7, 106–111. https://doi.org/10.1016/S1360-1385(01)02223-3

Jones, D.T., Taylor, W.R., Thornton, J.M., 1992. The rapid generation of mutation data matrices from protein sequences. Bioinformatics 8, 275–282. https://doi.org/10.1093/bioinformatics/8.3.275

Juang, K.-W., Lee, Y.-I., Lai, H.-Y., Wang, C.-H., Chen, B.-C., 2012. Copper accumulation, translocation, and toxic effects in grapevine cuttings. Environ Sci Pollut Res 19, 1315–1322. https://doi.org/10.1007/s11356-011-0657-3

Juang, K.-W., Lo, Y.-C., Chen, T.-H., Chen, B.-C., 2019. Effects of Copper on Root Morphology, Cations Accumulation, and Oxidative Stress of Grapevine Seedlings. Bull Environ Contam Toxicol 102, 873–879. https://doi.org/10.1007/s00128-019-02616-y

Kaur, N., Kaitheri Kandoth, P., 2021. Tomato bZIP60 mRNA undergoes splicing in endoplasmic reticulum stress and in response to environmental stresses. Plant Physiology and Biochemistry 160, 397–403. https://doi.org/10.1016/j.plaphy.2021.01.033

Kelloniemi, J., Trouvelot, S., Héloir, M.-C., Simon, A., Dalmais, B., Frettinger, P., Cimerman, A., Fermaud, M., Roudet, J., Baulande, S., Bruel, C., Choquer, M., Couvelard, L., Duthieuw, M., Ferrarini, A., Flors, V., Le Pêcheur, P., Loisel, E., Morgant, G., Poussereau, N., Pradier, J.-M., Rascle, C., Trdá, L., Poinssot, B., Viaud, M., 2015. Analysis of the Molecular Dialogue Between Gray Mold (*Botrytis cinerea*) and Grapevine (*Vitis vinifera*) Reveals a Clear Shift in Defense Mechanisms During Berry Ripening. MPMI 28, 1167–1180. https://doi.org/10.1094/MPMI-02-15-0039-R

Kimata, Y., Kimata, Y.I., Shimizu, Y., Abe, H., Farcasanu, I.C., Takeuchi, M., Rose, M.D., Kohno, K., 2003. Genetic Evidence for a Role of BiP/Kar2 That Regulates Ire1 in Response to Accumulation of Unfolded Proteins. MBoC 14, 2559–2569. https://doi.org/10.1091/mbc.e02-11-0708

Ko, D.K., Brandizzi, F., 2024. Dynamics of ER stress-induced gene regulation in plants. Nature Reviews Genetics 25, 513–525. https://doi.org/10.1038/s41576-024-00710-4

Ko, D.K., Brandizzi, F., 2021. A temporal hierarchy underpins the transcription factor–DNA interactome of the maize UPR. The Plant Journal 105, 254–270. https://doi.org/10.1111/tpj.15044

Koizumi, N., Martinez, I.M., Kimata, Y., Kohno, K., Sano, H., Chrispeels, M.J., 2001. Molecular Characterization of Two Arabidopsis Ire1 Homologs, Endoplasmic Reticulum-Located Transmembrane Protein Kinases. Plant Physiology 127, 949–962. https://doi.org/10.1104/pp.010636

Kretschmer, M., Kassemeyer, H. -H., Hahn, M., 2007. Age-dependent Grey Mould Susceptibility and Tissue-specific Defence Gene Activation of Grapevine Berry Skins after Infection by *Botrytis cinerea*. Journal of Phytopathology 155, 258–263. https://doi.org/10.1111/j.1439-0434.2007.01216.x

Ky, I., Lorrain, B., Jourdes, M., Pasquier, G., Fermaud, M., Gény, L., Rey, P., Doneche, B., Teissedre, P.-L., 2012. Assessment of grey mould (Botrytis cinerea) impact on phenolic and sensory quality of Bordeaux grapes, musts and wines for two consecutive vintages: Botrytis cinerea effect on grape and wine quality. Australian Journal of Grape and Wine Research 18, 215–226. https://doi.org/10.1111/j.1755-0238.2012.00191.x

Lai, Z., Wang, F., Zheng, Z., Fan, B., Chen, Z., 2011. A critical role of autophagy in plant resistance to necrotrophic fungal pathogens. The Plant Journal 66, 953–968. https://doi.org/10.1111/j.1365-313x.2011.04553.x

Li, C., Zhang, T., Liu, Y., Li, Z., Wang, Y., Fu, S., Xu, Y., Zhou, T., Wu, J., Zhou, X., 2022. Rice stripe virus activates the bZIP17/28 branch of the unfolded protein response signalling pathway to promote viral infection. Molecular Plant Pathology 23, 447–458. https://doi.org/10.1111/mpp.13171

Li, Z., Howell, S.H., 2021. Review: The two faces of IRE1 and their role in protecting plants from stress. Plant Science 303, 110758. https://doi.org/10.1016/j.plantsci.2020.110758

Liu, J., Chen, N., Chen, F., Cai, B., Dal Santo, S., Tornielli, G.B., Pezzotti, M., Cheng, Z.-M., 2014. Genome-wide analysis and expression profile of the bZIP transcription factor gene family in grapevine (Vitis vinifera). BMC Genomics 15, 281. https://doi.org/10.1186/1471-2164-15-281

Liu, J.-X., Srivastava, R., Che, P., Howell, S.H., 2007. Salt stress responses in Arabidopsis utilize a signal transduction pathway related to endoplasmic reticulum stress signaling: Salt stress

elicits ER stress response. The Plant Journal 51, 897–909. https://doi.org/10.1111/j.1365-313X.2007.03195.x

Liu, Y., Chen, Y., Li, B., Jing, Y., Tian, S. and Chen, T. (2025), Revisiting Endoplasmic Reticulum Homeostasis, an Expanding Frontier Between Host Plants and Pathogens. Plant, Cell & Environment, 48: 3281-3292. https://doi.org/10.1111/pce.15344

Martín, L., Millán, A., Castaño, F.J., Fontaine, F., 2023. Deciphering Chitosan–Host Plant Interaction in Esca Disease. Agronomy 13, 1290. https://doi.org/10.3390/agronomy13051290

Martins, V., Teixeira, A., Hanana, M., Blumwald, E., Gerós, H., 2015. Copper stress in grapevine, in: Gerós, H., Chaves, M.M., Gil, H.M., Delrot, S. (Eds.), Grapevine in a Changing Environment. Wiley, pp. 299–319. https://doi.org/10.1002/9781118735985.ch13

Mian, G., Musetti, R., Belfiore, N., Boscaro, D., Lovat, L., Tomasi, D., 2023. Chitosan application reduces downy mildew severity on grapevine leaves by positively affecting gene expression pattern. Physiological and Molecular Plant Pathology 125, 102025. https://doi.org/10.1016/j.pmpp.2023.102025

Mishiba, K., Iwata, Y., Mochizuki, T., Matsumura, A., Nishioka, N., Hirata, R., Koizumi, N., 2019. Unfolded protein-independent IRE1 activation contributes to multifaceted developmental processes in Arabidopsis. Life Sci. Alliance 2, e201900459. https://doi.org/10.26508/lsa.201900459

Moreno, A.A., Mukhtar, M.S., Blanco, F., Boatwright, J.L., Moreno, I., Jordan, M.R., Chen, Y., Brandizzi, F., Dong, X., Orellana, A., Pajerowska-Mukhtar, K.M., 2012. IRE1/bZIP60-Mediated Unfolded Protein Response Plays Distinct Roles in Plant Immunity and Abiotic Stress Responses. PLoS ONE 7, e31944. https://doi.org/10.1371/journal.pone.0031944

Nagashima, Y., Mishiba, K., Suzuki, E., Shimada, Y., Iwata, Y., Koizumi, N., 2011. Arabidopsis IRE1 catalyses unconventional splicing of bZIP60 mRNA to produce the active transcription factor. Sci Rep 1, 29. https://doi.org/10.1038/srep00029

Nakamura, M., Nozaki, M., Iwata, Y., Koizumi, N., Sato, Y., 2022. THESEUS1 is involved in tunicamycin-induced root growth inhibition, ectopic lignin deposition, and cell wall damage-induced unfolded protein response. Plant Biotechnology 39, 129–138. https://doi.org/10.5511/plantbiotechnology.21.1224a

Narula, K., Elagamey, E., Abdellatef, M.A.E., Sinha, A., Ghosh, S., Chakraborty, N., Chakraborty, S., 2020. Chitosan-triggered immunity to *Fusarium* in chickpea is associated with changes in the plant extracellular matrix architecture, stomatal closure and remodeling of the plant metabolome and proteome. The Plant Journal 103, 561–583. https://doi.org/10.1111/tpj.14750

Newman, M.-A., Sundelin, T., Nielsen, J.T., Erbs, G., 2013. MAMP (microbe-associated molecular pattern) triggered immunity in plants. Front. Plant Sci. 4. https://doi.org/10.3389/fpls.2013.00139

Nitsch, J.P., Nitsch, C., 1969. Haploid Plants from Pollen Grains. Science 163, 85–87. https://doi.org/10.1126/science.163.3862.85

Ozgur, R., Uzilday, B., Iwata, Y., Koizumi, N., Turkan, I., 2018. Interplay between the unfolded protein response and reactive oxygen species: a dynamic duo. Journal of Experimental Botany 69, 3333–3345. https://doi.org/10.1093/jxb/ery040

Palliotti, A., Poni, S., 2015. Grapevine under light and heat stresses, in: Gerós, H., Chaves, M.M., Gil, H.M., Delrot, S. (Eds.), Grapevine in a Changing Environment. Wiley, pp. 148–178. https://doi.org/10.1002/9781118735985.ch7

Parra-Rojas, J., Moreno, A.A., Mitina, I., Orellana, A., 2015. The Dynamic of the Splicing of bZIP60 and the Proteins Encoded by the Spliced and Unspliced mRNAs Reveals Some Unique Features during the Activation of UPR in Arabidopsis thaliana. PLoS ONE 10, e0122936. https://doi.org/10.1371/journal.pone.0122936

Pu, Y., Ruberti, C., Angelos, E.R., Brandizzi, F., 2019. AtIRE1C, an unconventional isoform of the UPR master regulator AtIRE1, is functionally associated with AtIRE1B in Arabidopsis gametogenesis. Plant Direct 3, e00187. https://doi.org/10.1002/pld3.187

Qiang, X., Liu, X., Wang, X., Zheng, Q., Kang, L., Gao, X., Wei, Y., Wu, W., Wu, W., Zhao, H., Shan, W., 2021. Susceptibility factor RTP1 negatively regulates Phytophthora parasitica resistance via modulating UPR regulators bZIP60 and bZIP28. Plant Physiology 186, 1269–1287. https://doi.org/10.1093/plphys/kiab126

Ramakrishna, C., Singh, S., Raghavendrarao, S., Padaria, J.C., Mohanty, S., Sharma, T.R., Solanke, A.U., 2018. The membrane tethered transcription factor EcbZIP17 from finger millet promotes plant growth and enhances tolerance to abiotic stresses. Sci Rep 8, 2148. https://doi.org/10.1038/s41598-018-19766-4

Ruijter, J.M., Ramakers, C., Hoogaars, W.M.H., Karlen, Y., Bakker, O., van den Hoff, M.J.B., Moorman, A.F.M., 2009. Amplification efficiency: linking baseline and bias in the analysis of quantitative PCR data. Nucleic Acids Research 37, e45–e45. https://doi.org/10.1093/nar/gkp045

Shang, J., Lehrman, M.A., 2004. Discordance of UPR signaling by ATF6 and Ire1p-XBP1 with levels of target transcripts. Biochemical and Biophysical Research Communications 317, 390–396. https://doi.org/10.1016/j.bbrc.2004.03.058

Silva, P.A., Silva, J.C.F., Caetano, H.D., Machado, J.P.B., Mendes, G.C., Reis, P.A., Brustolini, O.J., Dal-Bianco, M., Fontes, E.P., 2015. Comprehensive analysis of the endoplasmic reticulum stress response in the soybean genome: conserved and plant-specific features. BMC Genomics 16, 783. https://doi.org/10.1186/s12864-015-1952-z

Tajima, H., Iwata, Y., Iwano, M., Takayama, S., Koizumi, N., 2008. Identification of an Arabidopsis transmembrane bZIP transcription factor involved in the endoplasmic reticulum stress response. Biochemical and Biophysical Research Communications 374, 242–247. https://doi.org/10.1016/j.bbrc.2008.07.021

Takahashi, H., Kawakatsu, T., Wakasa, Y., Hayashi, S., Takaiwa, F., 2012. A Rice Transmembrane bZIP Transcription Factor, OsbZIP39, Regulates the Endoplasmic Reticulum Stress Response. Plant and Cell Physiology 53, 144–153. https://doi.org/10.1093/pcp/pcr157

Tamura, K., Stecher, G., Kumar, S., 2021. MEGA11: Molecular Evolutionary Genetics Analysis Version 11. Molecular Biology and Evolution 38, 3022–3027. https://doi.org/10.1093/molbev/msab120

Terrier, N., Glissant, D., Grimplet, J., Barrieu, F., Abbal, P., Couture, C., Ageorges, A., Atanassova, R., Léon, C., Renaudin, J.-P., Dédaldéchamp, F., Romieu, C., Delrot, S., Hamdi, S., 2005. Isogene specific oligo arrays reveal multifaceted changes in gene expression during grape berry (Vitis vinifera L.) development. Planta 222, 832–847. https://doi.org/10.1007/s00425-005-0017-y

Trdá, L., Fernandez, O., Boutrot, F., Héloir, M., Kelloniemi, J., Daire, X., Adrian, M., Clément, C., Zipfel, C., Dorey, S., Poinssot, B., 2014. The grapevine flagellin receptor Vv FLS 2 differentially recognizes flagellin-derived epitopes from the endophytic growth-promoting bacterium *Burkholderia phytofirmans* and plant pathogenic bacteria. New Phytologist 201, 1371–1384. https://doi.org/10.1111/nph.12592

Valente, M.A.S., Faria, J.A.Q.A., Soares-Ramos, J.R.L., Reis, P.A.B., Pinheiro, G.L., Piovesan, N.D., Morais, A.T., Menezes, C.C., Cano, M.A.O., Fietto, L.G., Loureiro, M.E., Aragão, F.J.L., Fontes, E.P.B., 2009. The ER luminal binding protein (BiP) mediates an increase in drought tolerance in soybean and delays drought-induced leaf senescence in soybean and tobacco. Journal of Experimental Botany 60, 533–546. https://doi.org/10.1093/jxb/ern296

Villette, J., Lecourieux, F., Bastiancig, E., Héloir, M.-C., Poinssot, B., 2024. New improvements in grapevine genome editing: high efficiency biallelic homozygous knock-out from regenerated plantlets by using an optimized zCas9i. Plant Methods 20, 45. https://doi.org/10.1186/s13007-024-01173-8

Wakasa, Y., Hayashi, S., Takaiwa, F., 2012. Expression of OsBiP4 and OsBiP5 is highly correlated with the endoplasmic reticulum stress response in rice. Planta 236, 1519–1527. https://doi.org/10.1007/s00425-012-1714-y

Walter, P., Ron, D., 2011. The Unfolded Protein Response: From Stress Pathway to Homeostatic Regulation. Science 334, 1081–1086. https://doi.org/10.1126/science.1209038

Wang, B., Du, H., Zhang, Z., Xu, W., Deng, X., 2017. BhbZIP60 from Resurrection Plant Boea hygrometrica Is an mRNA Splicing-Activated Endoplasmic Reticulum Stress Regulator Involved in Drought Tolerance. Front. Plant Sci. 8. https://doi.org/10.3389/fpls.2017.00245

Wang, J., Moeen-ud-din, M., Yin, R., Yang, S., 2022. ROS Homeostasis Involved in Dose-Dependent Responses of Arabidopsis Seedlings to Copper Toxicity. Genes 14, 11. https://doi.org/10.3390/genes14010011

Xu, Z., Song, N., Ma, L., Wu, J., 2019. IRE1-bZIP60 Pathway Is Required for Nicotiana attenuata Resistance to Fungal Pathogen Alternaria alternata. Front. Plant Sci. 10, 263. https://doi.org/10.3389/fpls.2019.00263

Yang, Y.-G., Lv, W.-T., Li, M.-J., Wang, B., Sun, D.-M., Deng, X., 2013. Maize Membrane-Bound Transcription Factor Zmbzip17 is a Key Regulator in the Cross-Talk of ER Quality Control and ABA Signaling. Plant and Cell Physiology 54, 2020–2033. https://doi.org/10.1093/pcp/pct142

Yang, Z.-T., Wang, M.-J., Sun, Ling, Lu, S.-J., Bi, D.-L., Sun, Le, Song, Z.-T., Zhang, S.-S., Zhou, S.-F., Liu, J.-X., 2014. The Membrane-Associated Transcription Factor NAC089 Controls ER-Stress-Induced Programmed Cell Death in Plants. PLoS Genet 10, e1004243. https://doi.org/10.1371/journal.pgen.1004243

Zapata, D., Salazar-Gutierrez, M., Chaves, B., Keller, M., Hoogenboom, G., 2017. Predicting Key Phenological Stages for 17 Grapevine Cultivars (*Vitis vinifera* L.). Am J Enol Vitic. 68, 60–72. https://doi.org/10.5344/ajev.2016.15077

Zhang, L., Zhang, C., Wang, A., 2016. Divergence and Conservation of the Major UPR Branch IRE1-bZIP Signaling Pathway across Eukaryotes. Sci Rep 6, 27362. https://doi.org/10.1038/srep27362

Zhu, J., Wang, G., Li, C., Li, Q., Gao, Y., Chen, F., Xia, G., 2019. Maize SEP15-like functions in endoplasmic reticulum and reactive oxygen species homeostasis to promote salt and osmotic stress resistance. Plant Cell & Environment 42, 1486–1502. https://doi.org/10.1111/pce.13507

Zuppini, A., Baldan, B., Millioni, R., Favaron, F., Navazio, L., Mariani, P., 2004. Chitosan induces Ca^{2+}-mediated programmed cell death in soybean cells. New Phytologist 161, 557–568. https://doi.org/10.1046/j.1469-8137.2003.00969.x

Figures

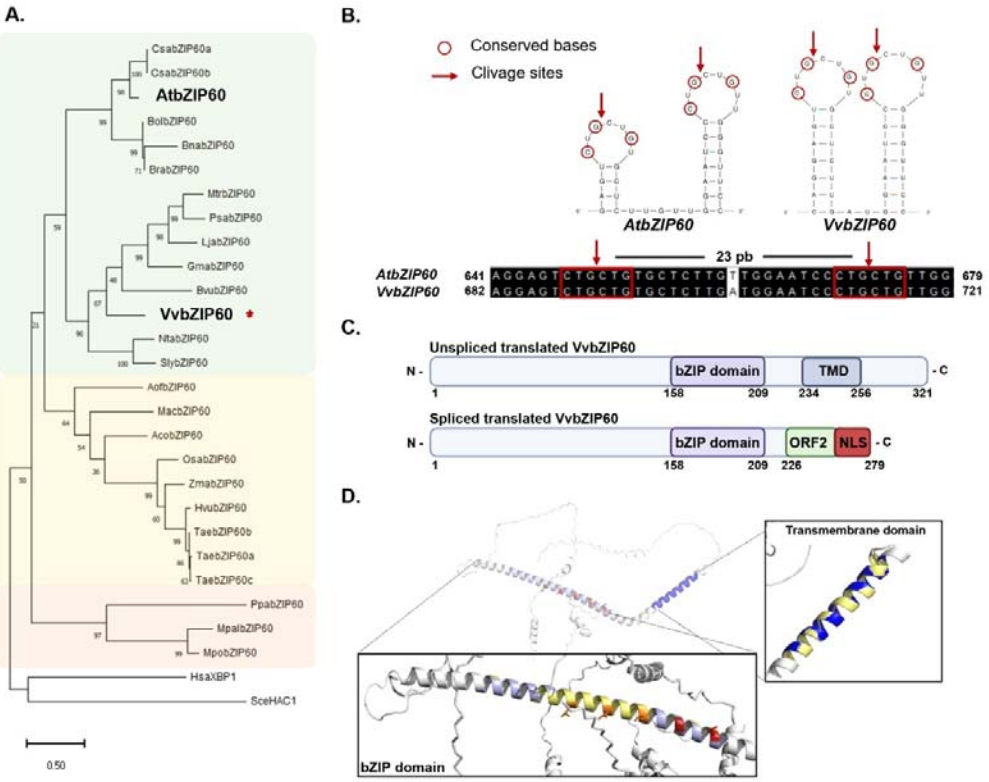

Fig. 1. Phylogenetic analysis of bZIP60 family. (A) Phylogenetic tree of bryophyte in orange, basal angiosperms monocotyledons (yellow) and dicotyledons (green) represented in different colors. The phylogenetic tree is rooted with human and yeast bZIP60 sequences. Red asterisk indicated *VvbZIP60* sequence. The phylogenetic tree was constructed using MEGA11 software with the maximum-likelihood method and a bootstrap consensus of 1,000 bootstraps. **(B)** Twin hairpin loop structure at splicing site in bZIP60 mRNA in *Arabidopsis thaliana* and *Vitis vinifera*. Each of the two loops contains three conserved bases (red rounds), also highlighted on the bZIP60 mRNA sequences in black. Red arrows indicate predicted cleavage sites. **(C)** Schematic representations of bZIP60 unspliced and spliced form predicted in silico. In purple, the bZIP domain, in blue the transmembrane domain (TMD) predicted by “DAS - Transmembrane Prediction server” (Cserzö et all. 1997), in green the open reading frame generated by the frame shift (ORF2) predicted by “ORF Finder” (Stothard 2000) and in red the nuclear signal predicted by “LOCALIZER” (Sperschneider J et al. 2017). **(D)** Structure prediction by “alphafold” of VvbZIP60. The bZIP domain and the transmembrane domain of *Vitis vinifera* in purple and blue are aligned with the one of *Arabidopsis thaliana* in yellow, in red/orange the 5 heptad Leucine and cysteine repeats.

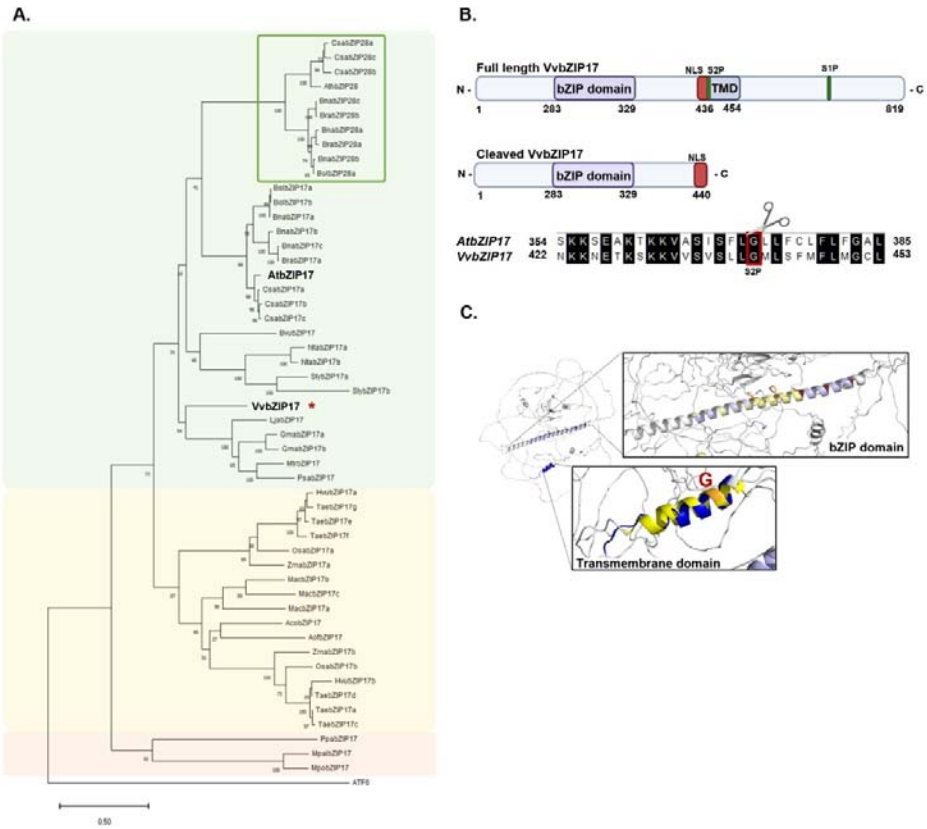

Fig. 2. Phylogenetic analysis of bZIP17/28 family. (A) Phylogenetic tree of bryophyte in orange, basal angiosperms, monocotyledons (yellow) and dicotyledons (green) represented in different colors. The phylogenetic tree is rooted with human ATF6 sequence. Red asterisk indicated VvbZIP17 sequence. Green border represent bZIP28 clade. The phylogenetic tree was constructed using MEGA11 software with the maximum-likelihood method and a bootstrap consensus of 1,000 bootstraps. **(B)** Schematic representations of bZIP17 before and after cleavage at S2P. In purple, the bZIP domain, in blue the transmembrane domain (TMD) predicted by “DAS - Transmembrane Prediction server” (Cserzö et all. 1997), in green the S2P and the S1P and in red the nuclear signal predicted by “LOCALIZER” (Sperschneider J et al. 2017). **(C)** Structure prediction by “alphafold” of VvbZIP17. The bZIP domain and the transmembrane domain of *Vitis vinifera* in purple and blue are aligned with the one of *Arabidopsis thaliana* in yellow, in red/orange the 5 heptad leucine and cysteine repeats. G in the transmembrane domain represent the clivage site S2P.

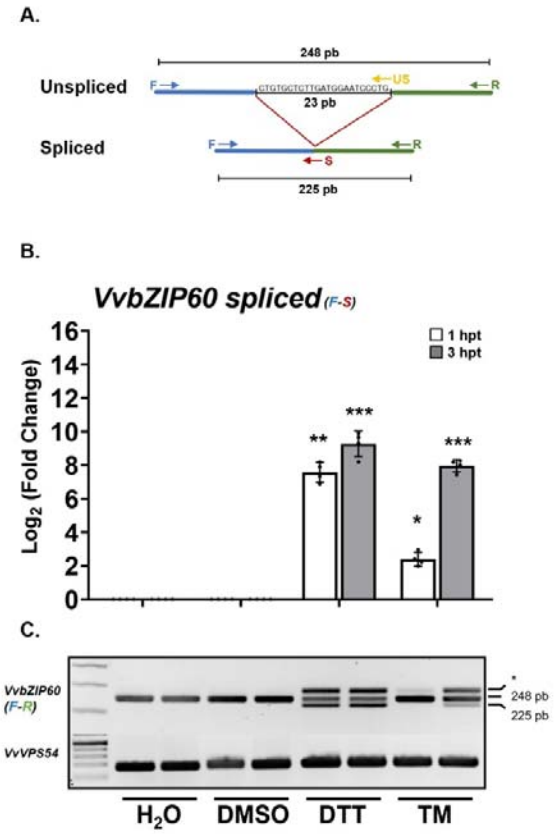

Fig. 3. Splicing assay of *bZIP60* in grapevine suspension cell. (A) Schematic representation of the primers used to amplify the spliced region of VvbZIP60 for the qRT-PCR and the primers used for semi-quantitative RT-PCR. F-S primers set for the putative splicing regions (red arrow) are indicated to amplify bZIP60s form. F-R sets are used to amplify the entire region covering the splicing site. **(B)** Log2-fold change values of *VvbZIP60 spliced* form measured by qRT-PCR 1- and 3-hours after 2 mM dithiothreitol (DTT), 0.2 µg/ml tunicamycin (TM) treatments and their respective negative control water and dimethyl sulfoxide (DMSO). Barplots represent the distribution of four independent biological repeats (n=4). Means of technical duplicates (efficiency-weighted Cq(w) values) were normalized using mean Cq(w) data of two housekeeping genes (*VvVSP54 and VvRPL18B*) before being analyzed. Asterisks indicate statistically significant differences between negative controls and the relative treatments using a ANOVA test followed by a TukeyHSD post doc test, ($P < 0.05$). **(C)** Semi-quantitative qRT-PCR analysis in agarose gel (3%) of *VvbZIP60* expression at 1 and 3 hpt in grapevine suspension cell treated as for (B). *VvVPS54* was analyzed as a loading control. PCR product sizes are indicated at right. Asterisk indicates a hybrid band formed by the bZIP60u and bZIP60s PCR products. Such hybrid band has been also observed and documented in RT-PCR analysis of XBP-1 and bZIP60 in *A. thaliana* (Shang and Lehrman, 2004; Moreno et al., 2012).

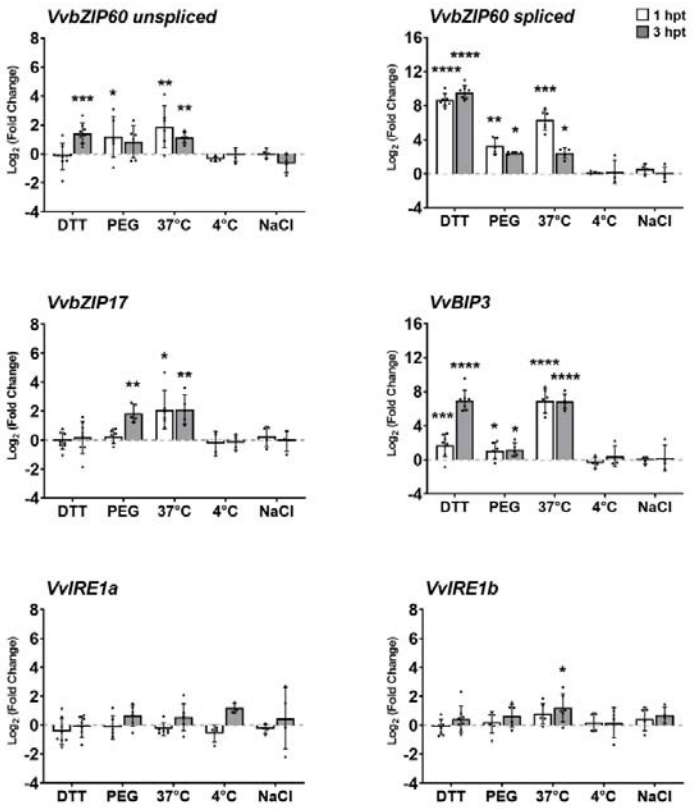

Fig. 4. Abiotic stress treatments trigger the expression of both UPR arms. Log2-fold change values of *VvbZIP60 unspliced* and *spliced* form, *VvbZIP17, VvBIP3, VvIRE1a* and *VvIRE1b* measured by qRT-PCR 1 – 3-hours after 2 mM dithiothreitol (DTT), 1% polyethylene glycol 8000 (PEG), 50 mM sodium chloride (NaCl), heat stress (37˚C) and cold stress (4˚C). Data represents the Log2-fold change of n > 4 independent biological repeats normalized on the negative control set at 0 (dot line). Means of technical duplicates (efficiency-weighted Cq(w) values) were normalized using mean Cq(w) data of two housekeeping genes (*VvVSP54* and *VvRPL18B*) before being analyzed. Data were converted in normal values through the “orderNorm transformation” (package: bestNormalize). Asterisks indicate statistically significant differences between negative control and the relative treatments using an ANOVA test followed by a TukeyHSD post doc test, ($P < 0.05$).

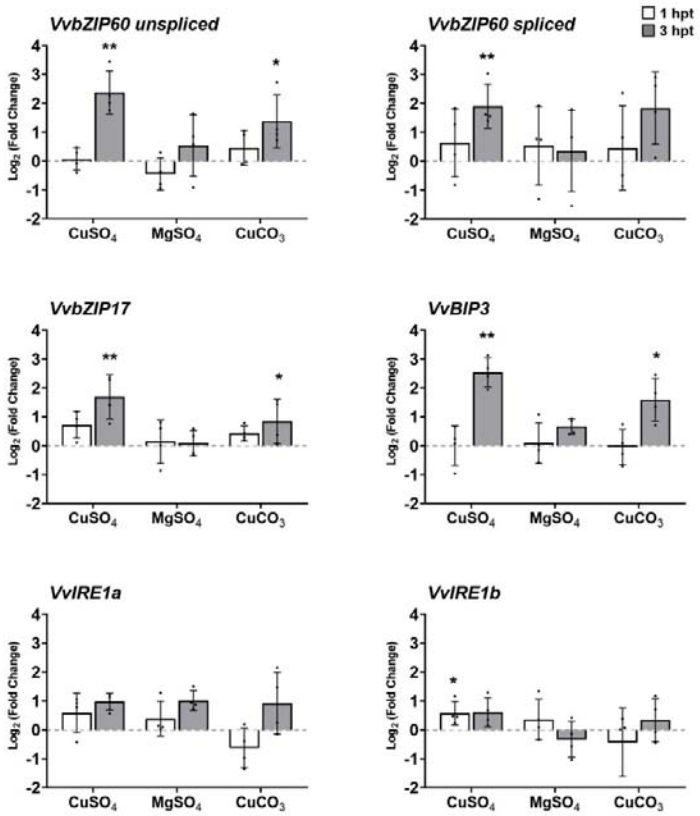

Fig. 5. Copper treatments trigger the expression of both UPR arms. Log2-fold change values of *VvbZIP60 unspliced* and *spliced* form, *VvbZIP17, VvBIP3, VvIRE1a* and *VvIRE1b* measured by qRT-PCR 1- and 3-hours after 0,1 mM copper(II) sulfate ($CuSO_4$), magnesium sulfate ($MgSO_4$), and copper(II) carbonate ($CuCO_3$). Data represents the Log2-fold change of four independent biological repeats (n=4) normalized on the negative control set at 0 (dot line). Means of technical duplicates (efficiency-weighted Cq(w) values) were normalized using mean Cq(w) data of two housekeeping genes (*VvVSP54* and *VvRPL18B*) before being analyzed. Data were converted in normal values through the “orderNorm transformation” (package: bestNormalize). Asterisks indicate statistically significant differences between negative control and the relative treatments at the same time point using an ANOVA test followed by a TukeyHSD post doc test, ($P < 0.05$).

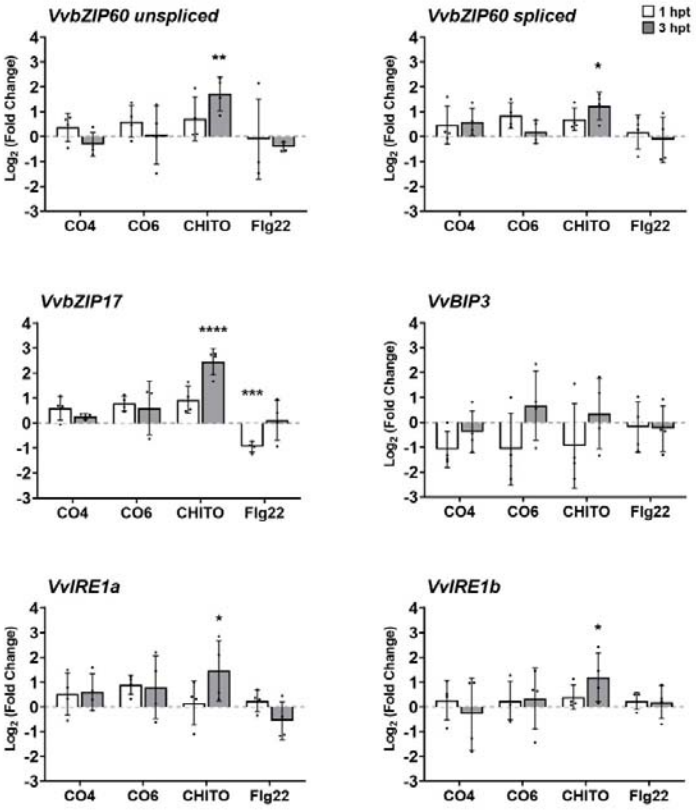

Fig. 6. Chitosan triggers the expression of both UPR arms. Log2-fold change values of *VvbZIP60 unspliced* and *spliced* form, *VvbZIP17* and VvBIP3 measured by qRT-PCR 1- and 3-hours after 0,2 mg/ml short-chitooligosaccharide DP4 (CO4), chitin DP6 (CO6), chitosan DP6 (CHITO) and 10^{-8} M flg22. Data represents the Log2-fold change of four independent biological repeats (n=4) normalized on the negative control set at 0 (dots line). Means of technical duplicates (efficiency-weighted Cq(w) values) were normalized using mean Cq(w) data of two housekeeping genes (*VvVSP54* and *VvRPL18B*) before being analyzed. Data were converted in normal values through the “orderNorm transformation” (package: bestNormalize). Asterisks indicate statistically significant differences between negative control and the relative treatments using an ANOVA test followed by a TukeyHSD post doc test, ($P < 0.05$).

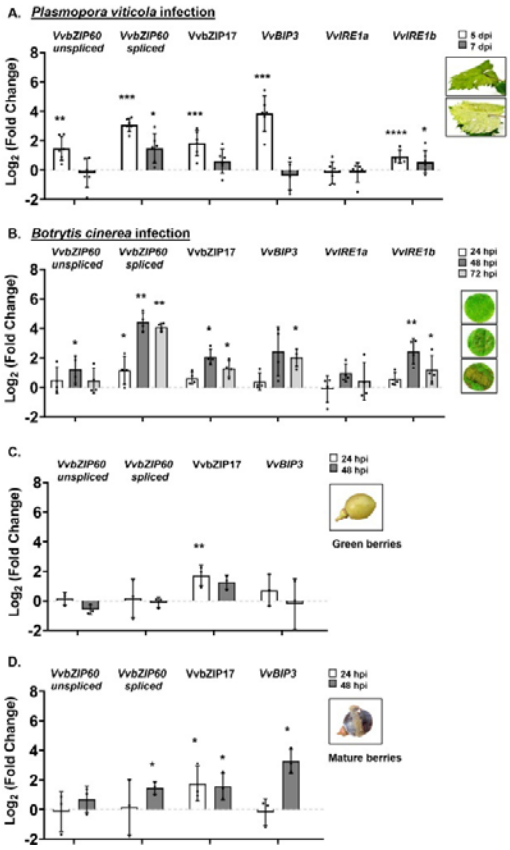

Fig. 7. *P. viticola* and *B. cinerea* trigger the expression of both UPR arms. **(A)** Log2-fold change values of *VvbZIP60 unspliced* and *spliced* form, *VvbZIP17, VvBIP3, VvIRE1a and VvIRE1b* measured by qRT-PCR 5-7-days post infection with *P. viticola* on grapevine leaves **(B)** Log2-fold change values of *VvbZIP60 unspliced* and *spliced* form, *VvbZIP17, VvBIP3, VvIRE1a and VvIRE1b* measured by qRT-PCR 24-48-72-hours post infection with *B. cinerea* on grapevine leaf disks. **(C-D)** Log2-fold change values of *VvbZIP60 unspliced* and *spliced* form, *VvbZIP17* and *VvBIP3* measured by qRT-PCR 24- and 48-hours post infection with *B. cinerea* on (C) green berries and (D) mature berries. Barplots represent the distribution of six, four and three independent biological repeats (n=6/n=4/n=3) respectively. Means of technical duplicates (efficiency-weighted Cq(w) values) were normalized using mean Cq(w) data of two housekeeping genes (*VvVATP16* and *VvEF1a*) before being analyzed. Asterisks indicate statistically significant differences between negative controls and the relative treatments at the same time point using an ANOVA test followed by a TukeyHSD post doc test, ($P < 0.05$).